Engineering an *In Vitro* Silk-Based Intestinal Model Using Topographical Features:

An investigation of the fabrication of silk fibroin based 3D scaffolds for the recreation of the surface topography (villi and crypts) of human small intestine

An Honors Thesis for the Department of Biomedical Engineering

By Megan W. Tse

Tufts University, 2018

Abstract

Millions of people worldwide are affected by intestinal diseases, which can severely affect people's quality of lives. Options to study intestinal functions and associated diseases are limited by existing models: cell co-cultures, microfluidic systems, organoid models, animal studies, and other in vitro systems. To replicate the in vivo functions of the intestines, we aimed to recreate the physical environment of the small intestinal niche through the incorporation of crypt- and villus-like structures in our current 3D tissue engineered intestinal model. With the goal of promoting the self-renewal of the intestinal epithelium, we seeded enteroids on patterned silk scaffolds. We aimed to look at the impact of the topographical features and the 3D geometry of the intestines of the intestinal epithelium formation and maturation. We've also used a novel method to create these topographical features through 3D printing, which is more efficient, quicker, and more cost efficient than the standard photolithography. In the further development of the model, we have demonstrated the ability of 3D printing to create villus- and crypt-like features. In addition, the possibility of incorporating these features in silk hydrogel and film coated silk sponges was also pursued. With initial seeding we have demonstrated the possibility of enteroids to adhere and proliferate to the featured silk hydrogel scaffolds and the formation of a polarized epithelial cell layer on the villus-like features. Through future works, we will be able to develop an *in vitro* physiologically relevant intestinal model that can be used for evaluating treatment cascades and screening orally delivered pharmaceuticals.

Acknowledgments

We thank the NIH (U19AI116497, P41EB002520) and the Gates Foundation for support of this work.

Table of Contents

List of Tables

List of Figures

1. Introduction

The understanding and treatment of gastrointestinal diseases presented a huge medical need globally. Intestinal diseases affected millions of people worldwide [1]. Although animal models existed, they failed to represent the same physiological responses in humans, resulting in improper modeling of intestinal diseases [2]. In addition to animal models, intestines have been modeled *in vitro* to replicate human intestinal conditions using 2D cultures of cell lines in Transwell inserts and complex 3D models with more than one cell type[3]. However, current *in vitro* models did not properly mimic the morphology of the luminal surface inside the human intestines. It was known that physical features of the tissue niche influence the formation of cells into tissues [3]. A silk-based 3D *in vitro* intestinal model from Chen et al. did mimic many qualities of the intestines, such as a gradient of oxygen, the potential to host bacteria, and a double layer of mucus lining the lumen supported by myofibroblasts [4].

One of the main issues with current *in vitro* models was the lack of physiological surface structures in the epithelium. The renewal of the intestinal epithelium, which is essential for intestinal functions, occurs with the replacement of epithelial cells with differentiated intestinal stem cells. These models were missing the representative topography of the intestines, which consists of a high density of villi and crypts, that likely guide differentiation[3]. It was shown that *in vitro* intestinal cells cultured on grooves and ridges would differentiate and spread in a more similar manner to *in vivo* intestinal cells, compared to flat surfaces[5]. To improve the silk-based intestinal model, silk scaffold geometry and topography were considered to optimize stem cell survival in crypt-like and

villus-like niches. In addition, another main issue was the use of cell lines. In order to recreate the self-renewal property, small intestinal organoids, enteroids, were used in the model as a variation of intestinal stem cells. With improvements made to the luminal surface of the silk-based model, the devised *in vitro* intestinal model was representative of the human intestinal tract, which can be used to study, understand, and treat intestinal diseases in the future. Microbiota and pathogens can be seeded in addition to the intestinal epithelial cells to address more of the cell to cell interactions. Investigators will not have to rely on *in vivo* models; this model may also serve as a more efficient screening test prior to initiating clinical trials for the treatment of intestinal diseases. The problem of severely limited tissue architecture will be overcome using this *in vitro* tissue system.

We aimed to develop a novel silk-based 3D *in vitro* intestinal model comprised of a unique topographical surface in the lumen similar to the *in vivo* intestines and formed by intestinal organoids. The addition of villi and crypts on luminal surfaces using silk in an *in vitro* 3D intestinal model was new. In order for intestinal stem cells to be able to properly differentiate on the scaffolds to form tissue, the morphology of the human intestines was recreated as much as possible in intestinal models. The intention of the project was to use silk as the scaffold with villi and crypts. Compared to other biomaterials, silk is biocompatible, slow in degradation, and mechanically robust. Innovative silk hydrogel scaffolds and sponges with villus-like and crypt-like surfaces were created for the intestinal model. In addition, many previous intestinal models with microscale geometries used photolithography to create high resolution molds. The use of

3D printing to create these features was novel. Also, the use of enteroids, small intestinal organoids, as stem cells in combination with the topographical feature allowed for the formation of the epithelium with tight junction and brush border formation. The novel, more representative *in vitro* intestinal model will allow for the ability to study, understand, and treat intestinal diseases resulting from cell to cell interactions with pathogens and probiotics.

2. Background

2.1. Human Small Intestines

2.1.1. General Anatomy

The small intestine is the primary digestive organ in the body, where most absorption occurs. It is approximately 3-5m in a living person with an approximate diameter of 2.5cm [6]. There are four tissue layers in the small intestines: outermost serosa, muscularis, submucosa, and mucosa. The inside wall of the intestines, mucosa, is highly folded with microscopic projections. Due to the many folds and projections within the small intestines, the small intestine on average has a surface area of approximately 200 square meters. The small intestine contains enzymes produced by the salivary glands, the pancreas, and the intestinal cells that aid in the process of carbohydrate, protein, and fat breakdown. Following breakdown, the enterocytes absorb the sugars, amino acids, and fatty acids with vitamins, salts, and water. The small intestine takes in 9 liters of water each day, absorbing approximately 7 liters. As an important digestive organ, abnormalities in the intestines can result in malabsorption of nutrients and diarrhea [6].

The small intestines are divided into 3 regions: duodenum, jejunum, and ileum. The duodenum is the shortest region and helps regulate the flow of bile and pancreatic secretions [6]. It is also where most chemical digestion takes place [7]. The jejunum is the middle section of the small intestines and is approximately 1m. The jejunum is designed to absorb carbohydrates and proteins. The jejunum's mucus membrane is covered in projections called villi to increase absorption. The epithelial cells along the villi contain microvilli, further increasing the surface area. The transport of nutrients includes the passive transport of carbohydrates and the active transport of amino acids, small peptides, vitamins, and glucose. The villi features in the jejunum are the longest in the small intestines. The ileum section is about 2m. The walls are thicker with more vasculature and mucosal folds than the jejunum [6]. The main function of the ileum is to absorb vitamin B12, bile salts, and other products of digestion. The ileum connects to the large intestine.

2.1.2. Topography of Intestinal Epithelium

The small intestinal lining consists of numerous densely packed villi and crypts throughout the surface of the lumen, which contribute to the enormous surface area. The crypts are well-like holes in between villi, which are finger-like protrusions. There are 20-40 villi per square millimeter [6]. The human small intestines has approximately one million crypts [8]. It is generally well known that mammalian cells respond to the physical and chemical properties of the microenvironment, the niche, surrounding the cells [3]. Intestinal stem cells lie at the base of the crypts and flow upwards, climbing the villi (Figure 1). As the stem cells leave the crypt, they differentiate into four main different types of intestinal epithelial cells [9]. The Paneth cells secrete antibacterial proteins and

exist both in the crypt and on the villi. The enterocytes are absorptive cells with a highly packed array of microvilli. These absorptive cells have large amounts of surface area that are important for absorption of nutrients in the intestines. The goblet cells secrete mucus to form the mucus lining in the intestines. The enteroendocrine cells secrete gut hormones. These gut hormones are a part of glucose homeostasis, pH balance, gall bladder contraction, gut motility, and the regulation of pancreatic and pituitary hormone secretion [8]. The combination of these four main cell types make up the intestinal epithelium, among other cell types [9]. When the intestinal Caco-2 cells were seeded on a polydimethylsiloxane (PDMS) substrate with a crypt-like pattern, the morphology and metabolic activity depended on the size of the crypts and the location relative to the crypts [10]. Thus, the differentiation, migration, and proliferation of the intestinal stem cells are likely dependent on the villi and crypt structures [10]. In consideration of further developing the model, seeding the intestinal stem cells on a luminal surface filled with crypts and villi will be necessary. As the intestinal stem cells proliferate and rise out of the crypts and along the villi, they differentiate. These cells eventually undergo apoptosis and are shed from the apex into the lumen [11]. Paneth cells are the exception to the upward migration pattern and remain near the crypt base [12]. This results in rapid turnover of the intestinal epithelium. In mammals, the epithelium undergoes turnover every 3-5 days [8]. Thus, recreating this self-renewal feature of the intestines will be important in recreating the function and structure.

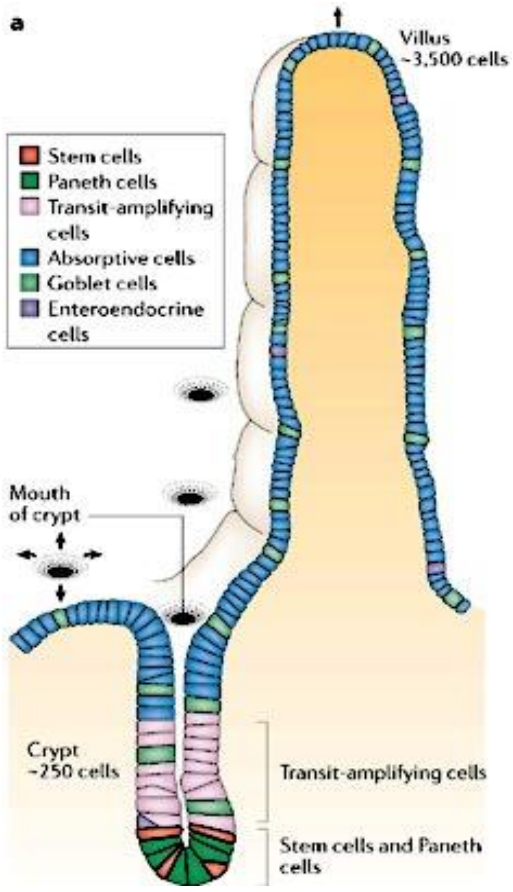

Figure 1. Intestinal Epithelium and Topography. The figure shows an example of the villus and crypt found densely packed on the epithelium, with the villus protruding into the luminal space of the intestines. In addition, the lining of the various cell types in which the intestinal stem cells differentiate into are shown rising out of the crypt and up along the villus, eventually shedding into the lumen. Most of the enterocytes, or absorptive cells, are along the villus. The Paneth cells are mostly located in the crypt with the transit-amplifying cells, which are derived from the intestinal cells. Transit-amplifying cells differentiate permanently into Paneth, enterocendocrine, goblet, or absorptive cells.

Image borrowed from "Organizing Stem Cell Renewal in Intestine: Stem Cells, Signals, and Combinatorial Control" [9]

2.1.3. Biochemical Gradient of Intestinal Epithelium

In addition to the presence of these topographical features, another important aspect of the intestines is biochemical gradient along these features. Intestinal stem cells proliferate and differentiate according to various signaling pathways. Paneth cells secrete factors that set up the gradients seen in the intestinal lining, indicating their importance in the intestinal stem cell maintenance [12]. The gradient of growth factors and receptors are oriented to facilitate proliferation or differentiation (Figure 2). There are three main pathways identified to be major contributors to the self-renewal feature of the intestines: Wnt-, BMP-, and Notch-pathways [12]. Wnts are ligands that regulate stem cell maintenance and differentiation. R-spondin factors are also known to enhance Wnt-

signaling and are a major contributor to the intestinal stem cell dynamics. Wnt gradients also regulate the cell compartmentalization and migration along the crypt-villus features [12]. BMP gradients are oriented in the opposite direction of Wnt gradients. BMP is known to reduce proliferation and increase differentiation as cells migrate from the bottom of the crypts [12]. BMP2 and BMP4 is secreted by the mesenchymal cells located within the villi and between the crypts [12]. BMP inhibitors, such as noggin, are mainly expressed in mesenchymal cells between the crypts. The combination of both BMP agonists and antagonists enable the intestinal self-renewal properties and differentiation [12]. Notch signaling is especially important for maintaining intestinal stem cells. In homeostasis, Notch causes the majority of epithelial cells to differentiate towards the absorptive cells. When Notch is reduced, intestinal stem cells reduce proliferation and differentiate towards a secretory cell fate, such as the Paneth, goblet, or enteroendocrine cells [12]. There is evidence that Notch may also regulate the Wnt-gradient influence, indicating the importance of interactions between the signaling pathways and factor gradients. Thus in the recreation of the small intestinal niche, the incorporation of these factors, in addition to the topography will play an important role.

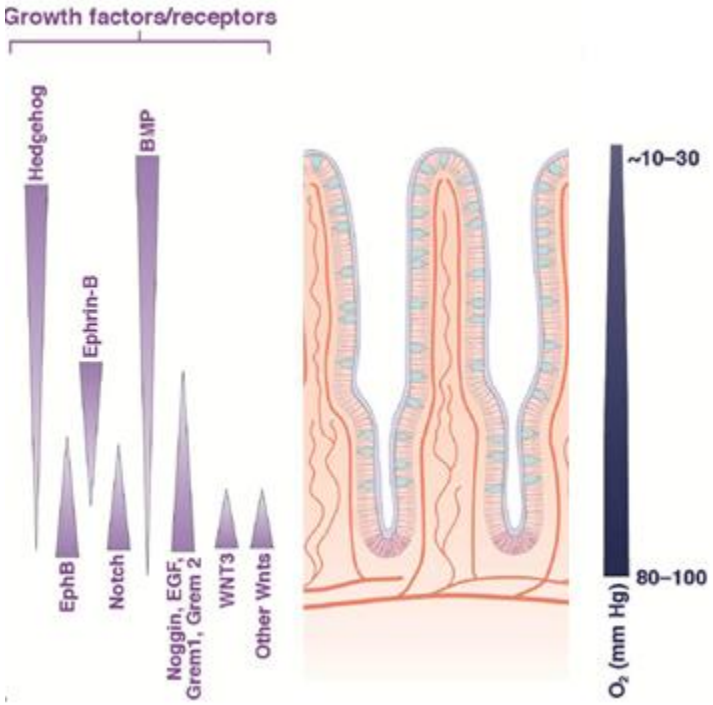

Figure 2. Small Intestinal Biochemical Gradient. The figure shows the biochemical gradient seen along the crypt-villus axis. The Hedgehog, BMP, Ephrin-B factors increase in concentration from the top of the villus to the bottom of the crypt. The EphB, Notch, Noggin, EGF, Grem1, Grem 2, Wnt3, and other Wnts decrease in concentration from the top of the villus to the bottom of the crypt. In addition, the oxygen gradient can be seen in this image, which decreases into the luminal space, from the crypt to the villus.

Image borrowed from "Bioengineered Systems and Designer Matrices that Recapitulate the Intestinal Stem Cell Niche" [12]

2.2. Intestinal Models and Associated Limitations

2.2.1. 2D Cell Cultures as Intestinal Models

To better understand absorption patterns and interactions of intestinal epithelial cells with pathogens, biomimetic tissue models were devised to be more cost efficient and convenient compared to *in vivo* models [13]. Many 2D intestinal models initially designed consisted of monolayers of intestinal epithelial cell types [13]. These cell types typically consisted of Caco-2 cells, which can form enterocytes, and HT29-MTX cells, which are most similar to goblet cells [4]. Several studies have used Caco-2 cells on plastic dishes. These 2D models simulate the epithelial intestinal barrier that limits molecular transport and can be used to analyze gut absorption [14]. These cancerous cell lines tend to be highly proliferative and inexpensive, making them useful for mechanistic studies or high-

throughput screening [15]. Although 2D modeling allowed for basic understanding of gut absorption, these models failed to reproduce other specific properties within the human intestine, such as mucus lining and columnar shapes [16]. They are limited in their complexity and low physiological relevance. Culturing these 2D models on Transwell inserts have aided in creating a slightly more complex, relevant system in which a basolateral and apical side can be distinguished. However, these systems are still limited due to their use of malignant cell lines.

2.2.2. 3D Intestinal Models

2.2.2.1. Gut-on-a-Chip Intestinal Model

Another model used is the gut-on-a-chip. In this model, Caco-2 cells were cultured within microfluidic channels of a PDMS mold (Figure 3). The cells were introduced to fluid flow and cyclic mechanical strain that was representative of the peristaltic motion in the intestines [16]. The result was the formation of villi, differentiation of intestinal cells, and elevated mucus production [16]. Although the microfluidic model more closely mimicked the human intestines compared to the 2D culture on Transwell inserts, the model does not

Figure 3. Gut-On-A-Chip Model. As seen from the scale of the finger, the model is relatively small and portable. The result of the microfluidic model was the formation of villi, as seen in the top right scanning electron microscopy image. In addition, there was the formation of the microvillus brush border around the Caco-2 cells, as seen with the bottom right image. The green represents the brush border and the blue represents the absorptive cells. The scale bar indicates a size of 25 microns.

Image borrowed from "Gut-on-a-Chip Microenvironment Induces Human Intestinal Cells to Undergo Differentiation" [16]

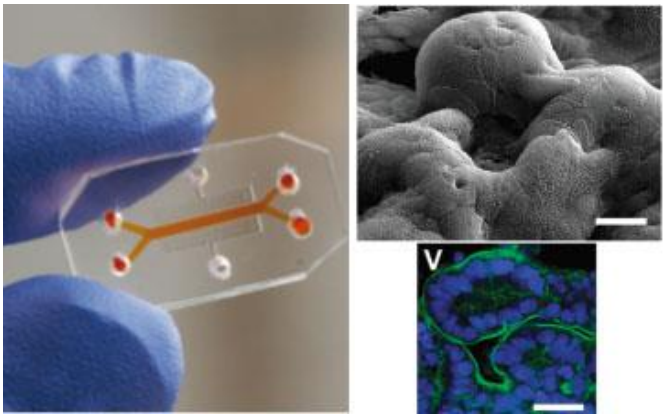

consider other qualities of the intestines such as the sophisticated topography, consisting of villi and crypts. This limited the representative niche of the intestines, preventing proper formation of the epithelium, and produced a relatively 2D model. The lack of stem cells also limited the tissue in replicating one of the key features of the intestines, the property of constant renewal.

2.2.2.2. Organoids Rotating Wall Vessel Model

In addition to the gut-on-a-chip model, an intestinal model consisting of enteroids on a rotating wall vessel exists. The rotating wall vessels bioreactor allows cells to grow and differentiate in 3D tissue-like assemblies (Figure 4) [17]. Using this assembly, mammalian cells and probiotics were cultured together in 3D. Intestinal enteroids were a significant improvement over the use of cancerous cell lines because they retained key features of the intestinal epithelium and formed the four different cell types and the crypt- and villus-like domains. The representation of an enteric disease model was also able to be created using intestinal enteroids with bacteria suspended in culture with the rotating wall vessels bioreactor; however, the topography of the intestines, consisting of continuous villi and crypts was poorly mimicked in all of the previously mentioned models. Due to the poorly mimicked topography, the intestinal epithelium was poorly formed, which did not allow for proper disease modeling.

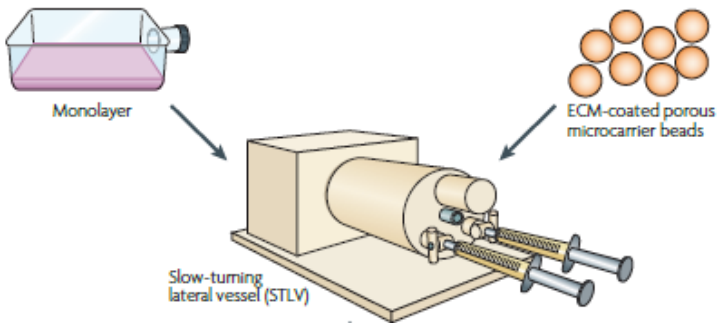

Figure 4. Organoid Rotating Wall Vessel Model. The operational principles of the rotating wall vessel technology is shown. Confluent monolayers are trypsinized and introduced into the slow-turning lateral vessel (STLV) together with porous microcarrier beads coated with extracellular matrix. Rotation of the STLV along a horizontal axis offsets sedimentation, causing gentle falling of the beads and cells through the culture medium within a restricted orbit, resulting in the establishment of three-dimensional tissue models.

Image and description borrowed from "Organotypic 3D Cell Culture Models: Using Rotating Wall Vessel To Study Host-Pathogen Interactions" [17]

2.2.2.3. PLGA Villi Intestinal Model

In order to address the issue of poorly formed topographies, a 3D intestinal model with villus features was assembled by Costello et al (Figure 5). Caco-2 and HT29-MTX cells were seeded on a porous PLGA intestinal scaffold coated with Matrigel [3]. The porous PLGA intestinal scaffold had an array of intestinal villi formed using laser ablation of PMMA and replica molding techniques. The villi were conically shaped, 500 μm in height, and 200 μm in diameter at the base. The porous scaffold allowed for epithelial cell attachment and proliferation. The spatial arrangement of cells was representative of the arrangement found in normal intestines with Paneth cells near the base and goblets cells migrated to the top of the villi. The model was able to more accurately represent the topography present in the human intestines compared to previous models. The model was also able to act as a disease model, showing attachment and degeneration of the microvilli as a result of the introduction of pathogens in addition to repair using

probiotics. However, the limitations associated with this model include the lack of the following: a double mucus layer, a gradient of oxygen content decreasing into the tissue, and the renewal of the epithelium.

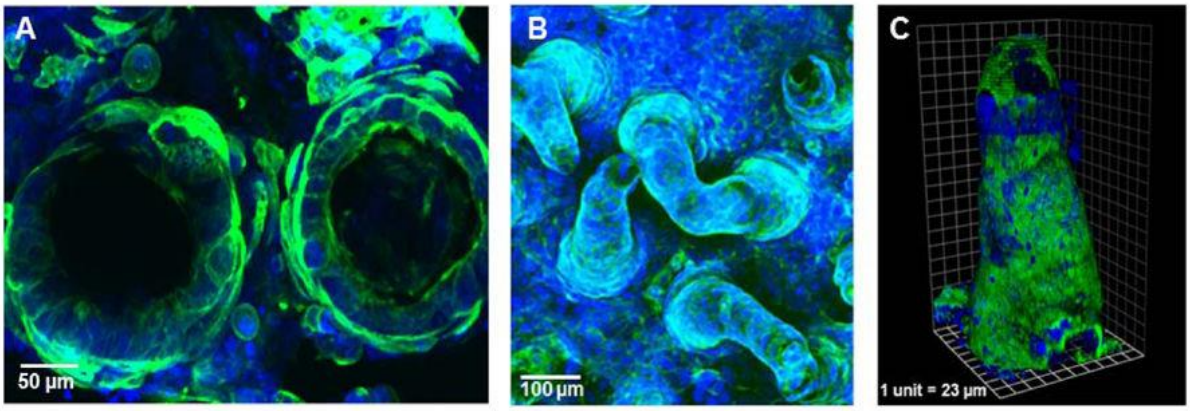

Figure 5. PLGA Villi Intestinal Model. The partial coverage of the Caco-2 and HT29-MTX cells can be seen in A) after 4 days. There is full coverage after 7 days as seen in B), indicating the cells are capable of proliferating up the villi features. 3D rendering seen in C) shows full coverage of cells on the 500um tall villi, which is within the range of physiological relevance. The blue is nuclei staining and the green is actin staining.

Image borrowed from "Synthetic small intestinal scaffold for improved studies of intestinal differentiation" [3]

2.2.2.4. Patterned Collagen Enteroid Model

To address the issue of a lack of self-renewal in intestinal models, Wang et al. devised a collagen scaffold with crypt-villus architecture (Figure 6). 1002F photoresist was used to create a master mold for PDMS stamps, which could create the features on collagen gels embedded in a Transwell insert [18]. Using differentiation media in the upper compartment and stem cell proliferation media in the lower compartment, a biochemical gradient of important signaling factors was created. This allowed to some extent, the proliferation of enteroids in the crypts and the migration of enteroids along the crypt-villus axis.

However, the model failed to properly demonstrate the differentiated epithelial cells were localized to the villi features and only indicated the presence of absorptive cells. In addition, there was a lack of characterization of the mucus layer, which is important in the recreation of the intestinal epithelium for disease modeling.

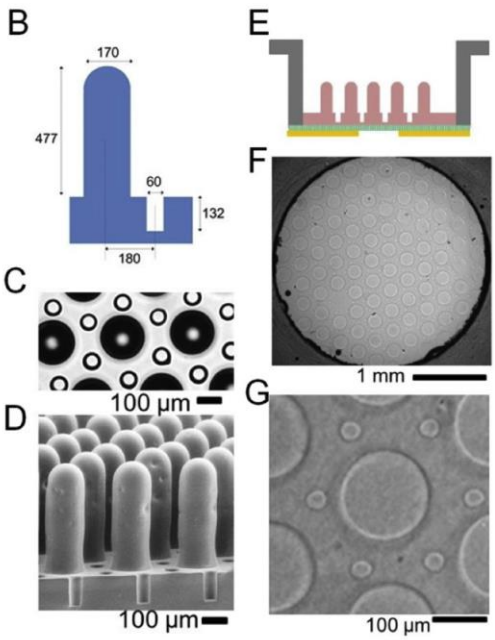

Figure 6. Patterned Collagen Enteroid Model. The micromolding schematic of the collagen scaffold on the Transwell can be seen in this model. The villi were approximately 500um in height and 170um in diameter. The crypts were about 130um tall and 60um in diameter, as seen in B). The top and side view of the first stamp used in the molding process can be seen in C) and D) from electron microscopy. The collagen scaffolds were molded onto an insert, which can be seen in E). The resulting patterned collagen on the insert can be seen in F) and G).

Image borrowed from "A microengineered collagen scaffold for generating a polarized crypt-villus architecture of human small intestinal epithelium" [18]

2.2.2.5. Silk Intestinal Model

2.2.2.5.1. Silk Pros/Cons

Silk is a naturally occurring polymer made by insects and worms [19]. Silk as a biomaterial is biocompatible, slow in degradation, and mechanically robust [20]. Silk is non-immunogenic and has already been FDA approved for use in some devices [21]. In addition, silk is capable of being solubilized and has already been used in various forms such as films, fibers, meshes, membranes, hydrogels, and sponges [19]. In these diverse forms as scaffolds, silk has shown its ability to support proliferation, differentiation, and tissue

repair [19]. Silk has also shown its ability to maintain long-term culture, particularly in adipose, bone, cortical brain tissue, kidney, and intestine engineering [22].

Although silk has many advantages particularly in the context of regenerative medicine, silk also has some disadvantages. Silk can add background noise in fluorescent imaging [22]. The background is due to tyrosine, tryptophan, and cross-links in silk that displays intrinsic fluorescence [23]. However, there have been algorithms developed to remove the noise associated with the fluorescence from silk [22]. In addition to autofluorescence, silk lacks selective cell binding sequences, requiring the use of other proteins to enhance cell attachment [22]. There have been methods developed to enhance binding such as incorporation of covalent decorations or RGD into silk [22].

2.2.2.5.2. Model Using Cell Lines: Caco-2 and HT29-MTX Cells

Utilizing silk's properties for tissue engineering, Chen et al. devised a 3D *in vitro* silk protein model with compartmentalized human intestinal tissue (Figure 7). The model was 8mm in length with a 5mm outer diameter and a 2mm inner diameter for the luminal space. Using smooth wires and screws, hollow channels with varying patterns were generated in the scaffold for the growth of Caco-2 and HT29-MTX cells [4]. Primary human intestinal myofibroblasts were seeded in the porous silk scaffold to support the formation of epithelium. The myofibroblasts secreted cytokines and growth factors to aid in the growth and differentiation of the epithelial cells [4]. The epithelial cells formed columnar structures and fully polarized epithelial cells had high packing density of microvilli [4]. The mucus layer formed in the system by HT29-MTX cells was substantially

thicker than normal 2D culture, which was significant in studying host-microbial interactions [24]. The mucus double layer formed was also more representative of the intestinal mucus layer with its adherent lower layer and looser upper layer. Similar to the human intestines, the mucus layer produced in this model formed a gradient of oxygen tension, decreasing in oxygen content the deeper into the epithelium and from the proximal to the distal end regions of the intestinal model [4]. This oxygen gradient is present in human intestines, which was not generally seen in 2D models and other 3D models. In addition, the tissue model indicated potential to support *in vitro* colonization of bacteria in the lumen. With further improvement to the system, intestinal function of the silk-based model will be enhanced.

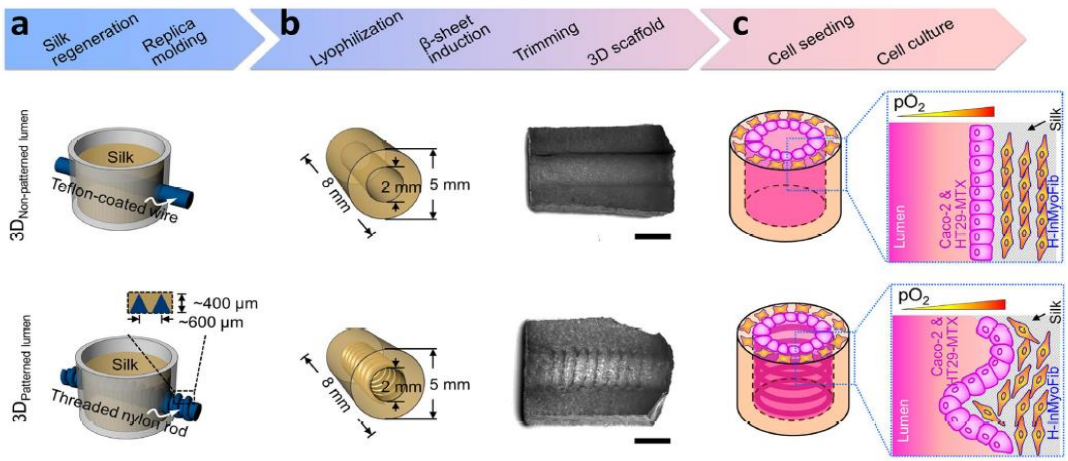

Figure 7. Process of Forming Human Intestines on 3D Porous Silk Scaffolds. The schematic of the fabrication process is shown in this image. Silk scaffolds were generated by regenerating silk, casting cylindrical PDMS, inserting a wire or screw to create the lumen, application of silk solution, lyophilization, and beta sheet induction. After trimming into 8mm pieces and removing the wire or screw, the scaffold was formed and cells were seeded on the scaffold to allow for the myofibroblasts to stay in the porous scaffold and the Caco-2 and HT29-MTX cells to be seeded on the surface of the lumen. The diameter of the cylinder was 5mm and the luminal space was 2mm in dimeter. From the diagram, the gradient of the oxygen content can be seen as described with greater oxygen tension farther into the epithelium.

Image borrowed from "Robust Bioengineered 3D Functional Human Intestinal Epithelium" [4]

2.2.2.5.3. Model Using Enteroids

In the previously mentioned model using cancerous cell lines, Chen et al. established a small intestinal tissue model that used a scaffold with a porous bulk and hollow luminal space. In a more recent model, stem cell-derived human intestinal small intestinal enteroids were seeded in the luminal space of the scaffold in place of the cancerous cell lines previously used (Figure 8) [25]. The bulk still contained intestinal myofibroblasts. The four major terminally differentiated epithelial cell types mentioned in section 2.1.2 were characterized. In addition, tight junction formation, microvilli polarization, digestive enzyme secretion, and low oxygen tension in the lumen was characterized in the model. The model was also able to respond to *E. coli* infection, displaying antibacterial responses. There was also potential seen in establishing an inflammatory bowel disease model using this system. However, the model lacked the demonstration of self-renewal seen in the intestines, which is key to the absorptive and protective functions of the intestines.

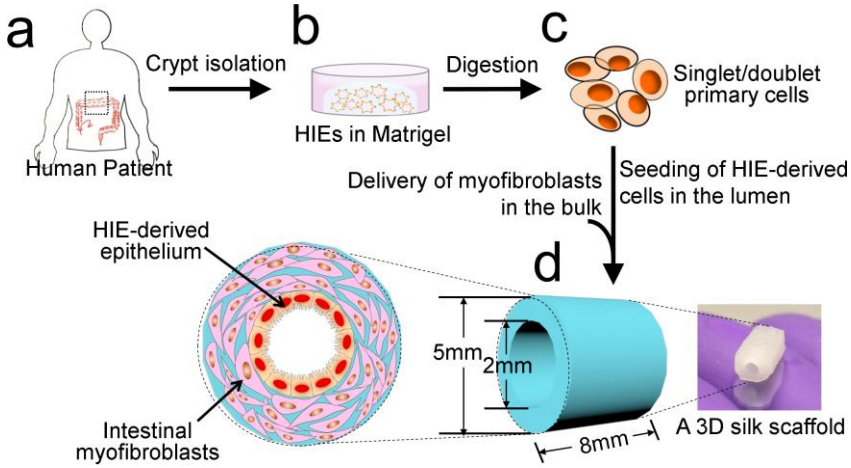

Figure 8. Process of Creating Enteroid Silk Intestinal Model. The enteroids are derived from human crypts and expanded in Matrigel. Following digestion of the enteroid clusters, single/doublet primary cells can be acquired and seeded as a monolayer. The intestinal myofibroblasts are seeded in the bulk while the enteroids are seeded in the lumen of the silk sponge scaffold. The scaffold used was similar to the model in section 2.2.2.5.2.

Image borrowed from "In vitro enteroid-derived three-dimensional tissue model of human small intestinal epithelium with innate immune responses" [25]

2.2.2.5.4. Silk Sponges vs. Silk Hydrogels

Previous attempts to incorporate features into the existing model have resulted in some issues [26]. One of the main concerns with the original model was the use of silk sponges. Although the use of silk sponges allow culture of other cell lines within the bulk, as indicated with the existing model, the pores created in lyophilized silk sponges typically range from approximately 100-400μm [27]. As we are trying to recreate the feature of self-renewal in the intestines and the average cell size is 10μm, there is a possibility that cells seeded on the silk sponge scaffold would proliferate into the pores.

Silk hydrogels can be formed through various methods: dehydration of solution, sonication, vortexing, decreased pH, surfactants, or electric fields [21]. These gels are formed by the induction of β-sheets. The β-sheets allow for the hydrogels to have

strength, structure, and long term stability; however, they also induce brittle behavior [21]. Another method to induce silk hydrogels is through enzyme catalyzed crosslinking of amino acid phenolic groups using horseradish peroxidase and hydrogen peroxide [21]. The technique is capable of forming hydrogels with controllable gelation kinetics and mechanical properties. The hydrogels can also be stiffened using β-sheet induction. The hydrogels were also determined to support cell proliferation and maintenance, in addition to being well tolerated *in vivo* [21]. Silk hydrogels have also been used to form high resolution features at 100μm, which is suitable for the construction of crypt-like and villus-like features [28].

2.3. Cell Lines Used in Intestinal Models

2.3.1. Common Cell Lines Used in Intestinal Models

The epithelium of the intestinal tract is constantly renewed, caused by the proliferation of intestinal stem cells from the bottom of the crypts to the top of the villi. The intestinal stem cells give rise to the intestinal epithelium cell types, which are important for the maintenance of the gastrointestinal homeostasis [29]. Although many of the models have used Caco-2 cells and HT29-MTX goblet cells, these are not practical to use in terms of creating a representative model with the appropriate physiological responses. Caco-2 cells are intestinal cancer cells, which are not appropriate to use for disease modeling purposes. They are derived from human colon adenocarcinoma and can undergo differentiation into a cell type similar to mature enterocytes [30]. Primary intestinal stem cells can be used, but do not exist in abundance and are costly.

2.3.2. Enteroids

2.3.2.1. Use of Enteroids in Silk Model

Therefore, for this project, we will be using small intestinal organoids, enteroids. Organoids are *in vitro* 3D clusters of stem cells acquired directly from the intestines of patients, which are capable of self-renewal and organization [31]. These organoids show the same functionality as their tissue of origin and rely on the extracellular matrix to facilitate self-organization. Organoids are more susceptible to the niche the cells are grown in, which include the growth factors and topographical features. In addition, intestinal organoid culture is capable of producing polarized 3D spheroid-like structures [32]. As indicated previously, enteroids are capable of differentiating into the four main intestinal cell type. There are two main methods for the acquisition of intestinal organoids: isolation of intestinal crypts with human adult stem cells and the use of human embryonic or induced pluripotent stem cells [32]. LGR5 has been used as an intestinal stem cell marker, particularly for the identification of intestinal stem cells derived from human crypts. LGR5+ stem cells have been demonstrated to differentiate into all small intestinal epithelial cells [11]. The major epithelial cell types found in enteroids, with similar proportions to human intestines, are the LGR5+ stem cells, Paneth cells, enteroendocrine cells, enterocytes, and goblet cells [32]. Therefore, in using enteroids for the *in vitro* human intestinal model, a more representative intestinal model that responds to the physiochemical environment will be developed.

2.3.2.2. Current Applications of Enteroids

The possibility of long term culture of enteroids has already been established in previous studies [33]. This system was capable of generating cultures from diseased tissues, making it valuable in studying diseased and normal gastrointestinal tissues. In addition, the enteroid culture has been used to study various gastrointestinal diseases already. It has been used to evaluate viral infections and host-pathogen interactions [34,35]. While the system is capable of studying intestinal diseases through infections and co-cultures, enteroids are also capable of being used in tissue engineering. Previously, enteroids were seeded on a patterned collagen gel and a silk sponge scaffold [4,18]. Thus, there is potential in tissue engineering to further establish physiologically relevant *in vitro* intestinal models.

2.4. Making Molds for Small Resolution Topographies

There are few possibilities to create the small resolution intestinal topography with densely packed villi and crypts. The villi are approximately 500-1000 μm tall with 100-500 μm sized circumference [36]. The crypts are in between the villi and intrude into the epithelium with approximately 250-500 micrometer depth and 50-500 micrometer sized circumferences [37].

One common method used in microfabrication is photolithography-based or soft lithography-based methods. Photolithography techniques are well established to form patterns on the scale of microns to millimeters [38]. This process typically requires UV exposure, multiple baking steps, and solvent deposition. In addition, there is generally a

high fabrication cost and cleanroom use needed especially in biological applications [38]. In addition to photolithography, soft lithography has been used as another common method for microfabrication. Soft lithography uses molding techniques to create replicas from a photo-defined mold [38]. The typical steps of soft lithography include the following: design of pattern, fabrication of master, fabrication of PDMS stamp, and soft lithography using microcontact printing, replica molding, or solvent-assisted micromolding [39]. However, this process still relies on cleanroom access to generate the photopatterned mold [38].

Following the initial testing of incorporating features, the morphology of the intestine-like surface was transferred to the *in vitro* model using either a master mold formed through micromachining or 3D printing.

2.4.1. Micromachining

Due to similarities in structures with microneedles, considerations for machining were made. The negative master molds were constructed using a computer numerical control (CNC) machining technique in a wax block [26]. Compared to cleanroom fabrication, this machining method was faster, allowed for quicker prototyping.

2.4.2. 3D printing

3D printing is the term used to describe the process of free form fabrication using a digital design file. This term encompasses bottom to top fabrication of material on a layer-by-layer basis. There are various methods for 3D printing including fused deposition modeling (FDM) and stereolithography (SLA). In addition to commercially

available printers with established software, custom printers are also being developed to accommodate various materials and possibilities in organ printing. Silk bioprinting was considered to form the surface; however, the resolution and accuracy needed for this project cannot be achieved through current techniques of customized 3D printing [40].

2.4.2.1. Fused Deposition Modeling

The FDM process forms 3D objects from a computer generated file. Typical programs to make these computer generated files include AutoCAD and Solidworks. FDM generally uses a heated extruder to expel a heated material. The extruder will move in the X or Y direction to deposit the semi-molten material layer-by-layer (Figure 9). After a layer is complete, the platform is typically lowered to create the next layer. The path and parameters are determined by the designer and depend on the material, the fabrication conditions, and design applications [41].

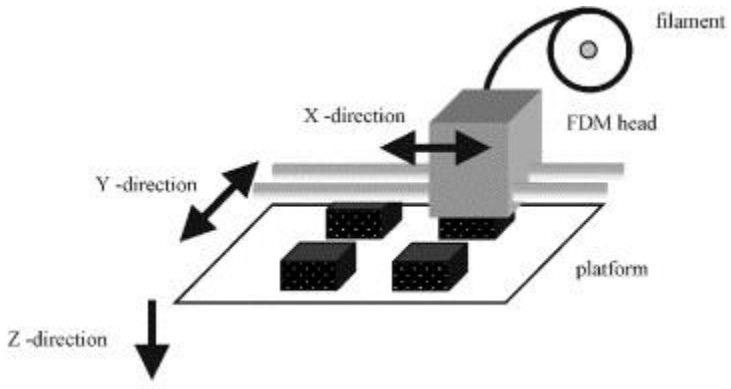

Figure 9. FDM 3D Printing Process. This is a schematic diagram of the FDM process. There is typically a filament that is melted and deposited by the FDM head. The head will move in the X or Y direction as the platform moves in the Z direction to form the 3D object desired. There is possibility to control the resolution by manipulating the layer thickness and the nozzle tip.

Image borrowed from "Fused Deposition Modeling of Novel Scaffold Architectures for Tissue Engineering Applications" [41].

2.4.2.2. Stereolithography

Stereolithography is the form of 3D printing that uses photopolymerization to create layers as opposed to the deposition of material. A source of light, such as a UV laser, can be used to induce crosslinking of photopolymers to form the bulk of the desired object. There are generally two methods in SLA printing: right-side up SLA and inverted SLA [42]. Right-side up SLA uses a large tank containing the photopolymer and platform. The UV laser comes from above and photopolymerizes the material to create a layer. The platform then descends and a blade filled with the photopolymer will recoat the platform with fresh material. Inverted SLA reverses the right-side up process (Figure 10). The layers are cured on a transparent, non-stick platform. Once the layer is complete, the build platform is lowered into a resin tank and leaves space equal to the layer height in between the build platform and the bottom of the tank. Once the light cures the resin on the platform, the platform moves up and the resin tank moves horizontally to separate the cured layer from the tank. More photopolymer flows into the tank to repeat the process. Compared to right-side up SLA printers, the price of inverted SLA printers is significantly less. Although the inverted SLA Form2 Printer from Form Labs have the disadvantages of a small build volume, it also has the advantages of easier use, affordability, lower maintenance, and easier material swapping potential. The Form2 is

also capable of high resolution printing compared to FDM printers. It produces 25µm layers, allowing it to be suitable for microscale modeling.

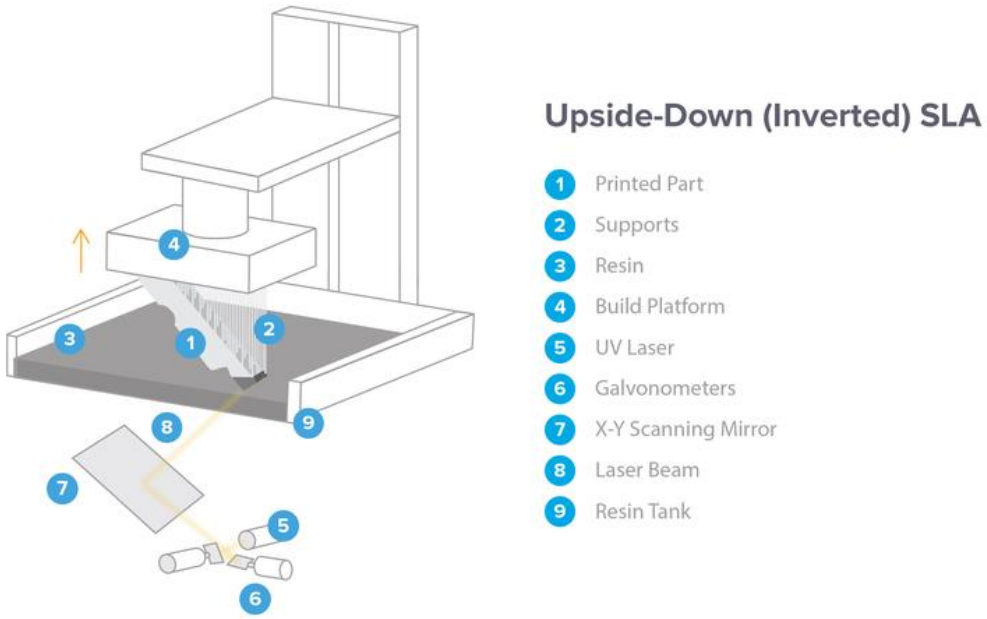

Figure 10. Step by Step Process for Inverted SLA Printing. The resin in this case is the photopolymer and the UV laser is the light source for polymerization.

Image borrowed from Form Labs website regarding SLA printing [42].

3. Research Objective and Project Aims

Intestinal diseases, such as inflammatory bowel disease and irritable bowel syndrome, affect millions of people worldwide [2]. In addition, acute enteritis, another intestinal disease, is the second leading cause of death worldwide [2,4]. Although these diseases affect millions, treatments are not as widely available to the world population due to the high costs of the treatments [2]. As a result, many intestinal models have been used to better understand and treat intestinal diseases to decrease costs and increase availability. However, animal models failed to portray the same physiological responses observed in humans, resulting in improper modeling [2]. Compared to *in vitro* models, animal models

were not nearly as controlled, making the possibility for disease and treatment studies limited. In addition, many of the current *in vitro* 2D models and 3D models did not appropriately reproduce *in vivo* intestines due to the improper niche of the models [3]. The niche includes the physical, chemical, and biological factors that affect the growth and development of cells in tissue formation. A 3D silk intestinal model was created by Chen et al., which accurately simulated many properties of the *in vivo* intestines, such as oxygen gradients, double mucus layer, and the ability to host probiotics [4]. The model used Caco-2 cells, which were derived from cancer patients. These cells cannot be implanted in humans due to their source, nor can they can be used to fully understand differentiation patterns in the intestines. A more recent model used human-derived small intestinal enteroids, which created a more physiologically relevant epithelium layer in the scaffold [25]. However, the intestinal model lacked a key feature needed to form the intestinal niche. This key feature was the topography for intestinal stem cells to form the epithelium. It is known that differentiation of stem cells into terminally differentiated adult cells depends on the physiochemical environment and niche [5]. Human intestines have densely packed villi protruding into the lumen and crypts intruding into the epithelium. Intestinal stem cells grow out of the crypt and differentiate as they rise up to the apex of the villus, indicating the importance of morphology. The complex interactions between probiotics in the human intestines and pathogenic bacteria and viruses cannot be properly mimicked and understood unless humans are used. This gap in knowledge prevents inexpensive, efficient studies for disease modeling, drug therapies, and absorption patterns in the intestines to be observed.

The long term objective is the development of a physiologically relevant in vitro 3D intestinal model to simulate disease and to create drug therapies for intestinal diseases. The specific objective of this project was to provide topographical features, such as densely packed villi and crypts, to recreate the intestinal niche on silk biomaterials to guide the differentiation and proliferation of enteroids. Our hypothesis was that by introducing closely packed villi and crypts, enteroids will differentiate from the crypts up along the villi, form the epithelium, increase mucus production, and improve tight junction formation. To test this hypothesis, we built upon the current model that exists by changing the surface of the lumen. We first aimed to fabricate topographical features on the silk scaffolds (Aim 1). Afterwards, we aimed to identify the effect of crypt-like and villus-like features of the lumen in the growth and development of the enteroids (Aim 2). The rationale for these studies was that they would lead to the development of an innovative, representative in vitro 3D model of the human intestines with more suitable cells in the epithelium to understand, study, and treat intestinal maladies.

4. Materials and Methods

4.1. Silk Solution Processing

Silk cocoons were turned into silk solution (Figure 11). 5g of silk cocoons was cut into pieces. Sericin was extracted by boiling the cocoons in 2L of 0.2% sodium carbonate for 30 or 60 minutes followed by three 20 minutes distilled water rinses. After washing the silk with water and drying for ~24 hours, the sericin-free silk was dissolved in 9.3M LiBr solution at 60°C for up to hours. The solution was then filtered using deionized water and cassettes with a 3500 molecular weight cutoff for three days to remove LiBr. After

centrifuging at 9000 rpm at 4°C for 20 minutes 2 times, the resulting solution was stored in 4°C.

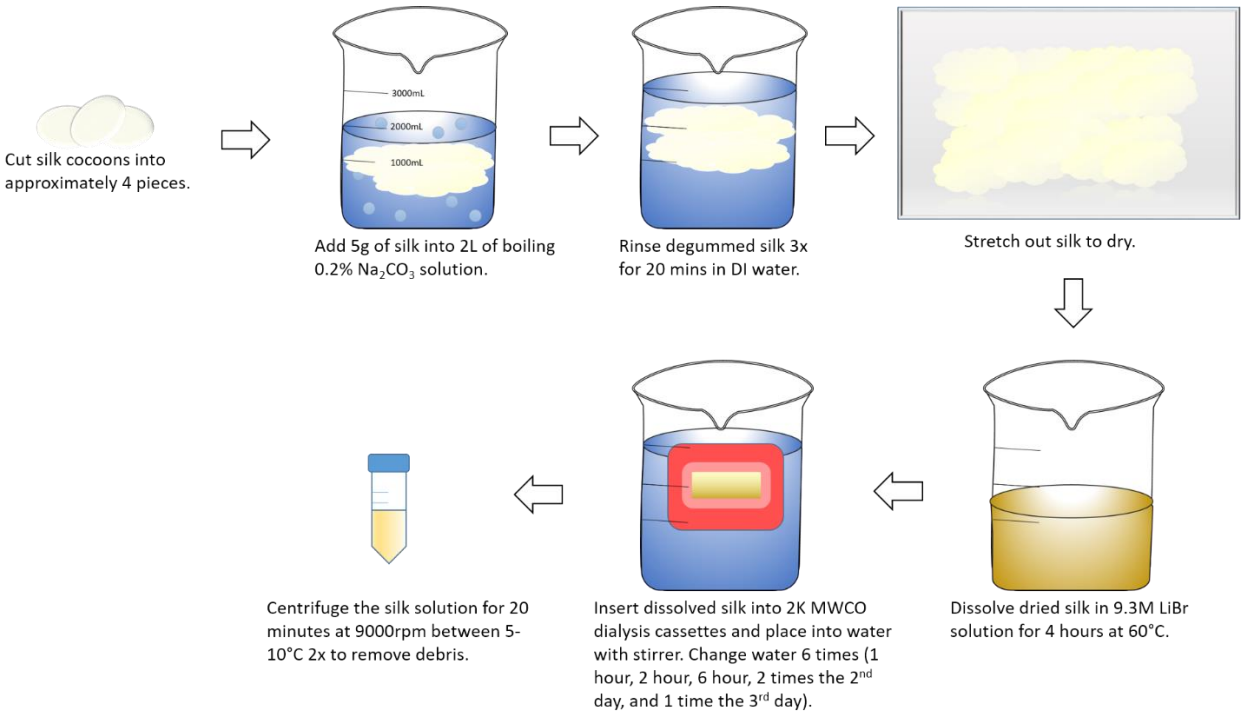

Figure 11. Silk Processing Schematic. This is the process of turning silk cocoons into silk solution.

4.2. Silk Hydrogel Fabrication

Silk hydrogels were made using the method previously described [43]. The hydrogels were made using 5% 60 minute boil silk, 2000 units/mL horse radish peroxidase (HRP), and 1% H_2O_2. The silk hydrogel solution was made by mixing silk, HRP, and H_2O_2 at a ratio of 10µL HRP: 10µL H_2O_2: 1mL silk solution. The PDMS molds were coated with 5% (w/v) pluronic F127 solution. Then, the silk hydrogel solutions were cast into the PDMS molds and heated at 37°C for 20-30 minutes. To make stiffer silk hydrogels, beta sheets were induced by autoclaving at 121°C for 30 minutes at 15 psi under a gravity cycle.

4.3. Silk Sponge Fabrication

5-6% 30 minute boil silk was casted into the rubber mold. The mold was placed in a desiccator overnight to create a film layer. The next day, the mold was placed in a water annealer for 2 hours to induce beta sheets. After cooling the water annealed films in -20°C for 30 minutes, 30 minute boil silk solution was casted quickly into the films. The solution was then frozen overnight (~12 hours) in -20°C. Then, the frozen silk was lyophilized at -80°C for 24-48 hours. Dry scaffolds were removed and autoclaved for beta-sheet induction. The scaffolds were autoclaved at 121°C for 30 minutes at 15 psi. Following autoclaving, the scaffolds were rehydrated in PBS and autoclaved under a liquid cycle at 121°C for 30 minutes at 15psi prior to use.

4.4. Design of Crypts and Villi Scaffolds in SolidWorks

The design of villus-like and crypt-like features was made using SolidWorks. For the positive master mold design, the villus features were extruded conical shaped features and the crypt features were conical shaped cuts. For the negative master mold design, the villus like features were conical shaped wells and the crypt features were extruded conical shaped features. The features created using micromachining and 3D printing can be seen in Table 1. The drawings for the master molds can be seen in Appendices A-D.

Table 1. Master Mold Dimensions					
Machined or Printed	*Villus Height (um)*	*Crypt Depth (um)*	*Diameter of Features (um)*	*Spacing Between Features (um)*	*Angle (Degrees)*
Machined	500	N/A	250	500	7.5
Printed	500	300	300	600	4
Printed	500	500	500	1000	4
Printed	800	700	500	1000	4

4.5. Method for Making Featured Scaffolds

The method for fabricating the silk hydrogel and silk sponge scaffolds with villi and crypts will be described in the results section (5.1 and 5.2).

4.6. Cell Culture of Caco-2 Cells

The Caco-2 (CRL-2102) cell line was obtained from ATCC (Rockville, MD). The culture media for Caco-2 consisted of DMEM (Gibco 10569010) supplemented with 10% FBS, 10µg/mL human transferrin (Invitrogen), and 1% Pen/Strep. The frozen vials were rapidly thawed in a 37°C water bath, neutralized with culture media, pelleted, and cultured by the following methods. The vials were warmed until 25% ice remained. After washing the cells with the culture media (ratio of 1mL into 9mL), the cells were pelleted in a 15mL falcon tube at 1200rpm for 5 minutes. Afterwards, the supernatant was removed and the cells were resuspended in 5mL media. The cell suspension was added to

a T-175 flask and an additional 15mL of media was added. The flask was kept in a 37°C incubator with 5% CO_2 and the media was changed every 2-3 days.

When the cells were confluent, the Caco-2 cells were passaged at a ratio of 1:6. After aspirating the old media, the cells were rinsed with 10mL of PBS. Following the removal of the PBS, 7.5mL of room temperature 0.25% trypsin-EDTA was added to the flask. The flask was then incubated for 10 minutes at 37°C to detach the cells from the flask. The cells were then pipetted up and down 10 times to detach the cells. The trypsin was neutralized using 10mL of media. The solution was mixed and placed into a 50mL falcon tube. The cells were centrifuged at 1200rpm for 5 minutes. After aspirating the supernatant, 30mL media was added and mixed. 5mL of the cell suspension was put into a new T-175 flask and 10mL media was added to the flask. The cells were then fed every 2-3 days until confluent and passaged again.

4.7. Seeding of Caco-2 Cells

When the cells were confluent, the Caco-2 cells were seeded on the scaffolds. The cells were digested using 0.25% trypsin-EDTA for 10 minutes, similarly to the passaging process in section 4.6. The cells were resuspended in 5mL media and counted using a hemocytometer. Briefly, 20uL of the cell suspension was added to the hemocytometer and counted. The cells were then diluted to the desired concentrations. Using 20uL drops, the cells were seeded on the flat scaffolds with and without features placed in a 24 well plate. To allow the cells to attach, the scaffolds were incubated for 1 hour before adding 1.2mL media per well.

4.8. Cell Culture of Enteroids

4.8.1. Jejunum and Ileum Enteroid Media Components

For jejunum cells, CMGF+ media was used. For ileum cells, high-wnt media was used. The CMGF- media consisted of 500mL Advanced DMEM/F12, 5mL 100X GlutaMAX, 5mL HEPES 1M, and 5mL 5000units/mL Penicillin/Streptomycin (Gibco 15070063). The CMGF+ media used to culture the jejunum enteroids consisted of Advanced DMEM/F12, 2mM GlutaMAX-I (Invitrogen 35050-061), 1x Penicillin/Streptomycin (Invitrogen 15140-122), Wnt (from cell lines), R-spondin (from cell lines), Noggin (from cell lines), 1x N2 supplement (Invitrogen 17502-048), 1x B27 supplement (Invitrogen 17504-044), 1mM N-Acetylcysteine (Sigma-Aldrich A9165-5G), 50ng/mL mouse recombinant EGF (Invitrogen PMG8043), 500nM A83-01 (Tocris 2939), 10uM SB202190 (Sigma-Aldrich S7067), 10mM Nicotinamide (Sigma-Aldrich N0636), 10nM [Leu15]-Gastrin I (Sigma-Aldrich G9145), and 10mM HEPES 1M (Invitrogen 156030-080). To make 500mL of CMGF-, the quantities and concentrations can be seen in Table 2. To make 40mL of CMGF+, the quantities and concentrations can be seen in Table 3. To make 40mL of the High-Wnt media, the quantities and concentrations can be seen in Table 4.

Table 2. CMGF- Components

Item	*Quantity for ~500mL*
Advanced DMEM/F12 (Invitrogen)	500mL
Glutamax 100x (Invitrogen, final conc 1X)	5mL
HEPES 1M (Invitrogen, final conc 10mM)	5mL
Penicillin/Streptomycin 10000 units/mL (Invitrogen, final conc 100 units/mL)	5mL

Table 3. CMGF+ Media Components	
Item	*Quantity for 40mL*
CMGF-	6mL
Wnt Media	20mL
R-Spondin Media	8mL
Noggin Media	4mL
B27 50X	800µL
N2 100X	400µL
Nicotinamide 19mM	400µL
N-acetylcysteine 500mM	80µL
Primocin 50mg/mL	80µL
EGF 1000X	40µL
Gastrin 1000X	40µL
A83 1000X	40µL
SB202190 1000X	40µL

Table 4. High-Wnt Media Components	
Item	*Quantity for 40mL*
CMGF+	20mL
Wnt Media	20mL
Primocin (50mg/mL)	40µL

4.8.2. Culture of L Wnt-3A Cells

From a vial of L Wnt-3A cells, similar to the thawing process in section 4.6, the cells were resuspended in 4mL of Wnt growth medium, as seen in Table 5 and distributed to 4 T-75 flasks. Then 14mL growth media was added. The cells were fed every other day.

After the cells were confluent, the 4 flasks were passaged into 10 T-75 flasks. Briefly, each of the 4 confluent flasks received 4mL of 0.25% trypsin-EDTA. After 1 minute in room temperature, the cells became detached. The trypsin was neutralized in a 50mL conical tube with 5mL of special antibiotic-free medium and centrifuged at 200g for 5 minutes. After aspirating the supernatant, the cells were resuspended in 10mL of conditioning medium. 9 T-75 flasks received 1mL of the cell suspension with conditioning medium. The rest was re-pelleted and replaced with 1mL of Wnt growth

medium, which was dispensed into 1 T-75 flask. An additional 9mL of conditioning medium was added to the flasks with conditioned medium. An additional 14mL was added to the flask with growth medium.

After 4 days, the first harvest of the Wnt media was obtained from the 9 T-75 flasks with conditioning medium. The media was removed and centrifuged at 1000g for 10 minutes. Then, the media was sterilized and stored. An additional 10mL of conditioning medium was added to each flask and the cells were cultured for another 3 days. After 3 days, the Wnt media was obtained, centrifuged, and filtered for the second harvest. The first and second harvest Wnt media was mixed and stored. The growth flask was used to repeat the process.

4.8.3. Culture of 293T-HA-Rspol-Fc Cells

For the culture of 293T-HA-Rspol-Fc cells, the process was similar to section 4.8.2. The various media can be found in Table 5. However, a diluted concentration of 0.25% trypsin-EDTA was used. The concentration was diluted 1:3 using PBS. After the 4 flasks became confluent, the cells were split 4:5. 4 T-75 flasks received 15mL of special antibiotic free medium. 1 T-75 flask received 15mL of R-spondin growth medium. After these 5 flasks became confluent, the 4 T-75 flasks with antibiotic free medium were passaged again into 10 T-75 flasks with 20mL of conditioning medium. The 1 T-75 flask with R-spondin growth medium was passaged to repeat the culturing process. The R-spondin media was collected after 1 week.

4.8.4. Culture of 293-Noggin Cells

For the culture of 293-Noggin cells, the process was similar to section 4.8.3. Rather than using the R-spondin growth medium, Noggin growth medium was used. The components for the Noggin growth medium can be seen in Table 5.

Table 5. Various Media Used in Culturing Cell Lines for Enteroid Medium

Medium Type	Components	Quantities for ~500mL
Wnt Growth	DMEM (Gibco 10569010)	450mL
	FBS (final conc 10%)	50mL
	G-418 (final conc 400µg/mL)	4mL
	Pen/Strep (final conc 1X)	5mL
R-Spondin Growth	DMEM (Gibco 10569010)	450mL
	FBS (final conc 10%)	50mL
	Zeocin (final conc 300µg/mL)	1.5mL
	Pen/Strep (final conc 1X)	5mL
Noggin Growth	DMEM (Gibco 10569010)	450mL
	FBS (final conc 10%)	50mL
	Puromycin (final conc 10µg/mL)	500µL
	Pen/Strep (final conc 1X)	5mL
Special Antibiotic Free	DMEM (Gibco 10569010)	450mL
	FBS (final conc 10%)	50mL
	Pen/Strep (final conc 1X)	5mL
Conditioning	Advanced DMEM/F12 (Invitrogen)	450mL
	FBS (final conc 10%)	50mL
	Glutamax (final conc 1X)	5mL
	Pen/Strep (final conc 1X)	5mL

4.8.5. Thawing, Maintaining, Passaging Enteroids

A frozen vial was obtained from the liquid nitrogen tank. The vial was thawed in room temperature water until 50% frozen. The cell suspension was removed from the vial and mixed with 4.5mL of cold CMGF- in a 15mL tube. The cell was centrifuged at 200g for 5 minutes at 4°C. The supernatant was then aspirated. Matrigel was added to the solution (1 vial into 4 wells with 2 15µL droplets). Using a 24 well plate, 2 15µL droplets were placed in each well. After 2 minutes in room temperature, the plate was flipped upside

down and incubated for 7 minutes. The enteroids were then resuspended in 500µL of media per well. The enteroids were fed every other day.

After approximately 1 week (or when confluent), the enteroids were passaged at a ratio of 1:3. After aspirating the old media and replacing it with cold CMGF-, a cell scraper was used to break up the Matrigel droplets. Using a P1000 pipette, the Matrigel was pipetted up and down 10 times to further break the gel. A 1mL 25G syringe was then used to break up the cells into smaller clusters. The solution was drawn up and released 5 times. Afterwards, the cell suspension with Matrigel was centrifuged at 200g for 5 mins at 5°C. The supernatant was aspirated and the enteroids were resuspended in Matrigel to be plated, similarly to the thawing step with 2 15µL droplets per well.

4.9. Seeding of Enteroids

Prior to seeding enteroids on the scaffolds, a collagen coating was required. Briefly, collagen type I was diluted to make a 50µg/cm^2 coating on the scaffolds. The solution was applied and left overnight in 4°C. After rinsing 3 times with 1X PBS every 2 hours, the coated scaffolds were used for seeding.

Approximately 1 well was used per scaffold. The wells were washed with 500µL of cold 0.5mM EDTA. The Matrigel droplets were broken up using a P1000 pipette and pipetted up and down 10 times. The solution was centrifuged at 200g for 5 minutes at 4°C. The EDTA wash was removed and the enteroids were dissociated with 500µL of 0.05% trypsin-EDTA per well at 37°C for 4 minutes. After 4 minutes, equal amounts of CMGF-

with 10% FBS was added and mixed using P1000 50 times. The solution was then put through a 40um cell strainer and the cell strainer was rinsed with additional CMGF- with 10% FBS. The cell suspension was spun at 1500rpm at room temperature for 5 minutes. The supernatant was aspirated. The cell pellet was resuspended in media with 10µM Y-27632. 20µL of media was deposited on each 2D scaffold and 30µL of media was deposited onto each 3D scaffold. After the cells were incubated on the scaffold in the form of a droplet for 1 hour, 500µL of media with 10µM Y-27632 was added to each well. Every other day, the media was replaced with 500µL of media.

4.10. Methods of Evaluation

4.10.1. Scanning Electron Microscopy

The scaffolds were fixed with 1% glutaraldehyde in PBS at room temperature for 1 hour. Afterwards, the scaffolds were rinsed using PBS at 4°C for 30 minutes. Then, the scaffolds were rinsed with water at 4°C for 15 minutes twice. Following this water rinse, another set of water rinse was done at 0°C three times for 10 minutes each. Afterwards, a series of dehydration treatments using various concentrations of ethanol was done. The scaffolds were dehydrated in 50% ethanol on ice for 1 hour, 90% ethanol in -20°C for 1 hour, 100% ethanol in -20°C for 1 hour, and 100% ethanol in 20°C overnight. The samples were then rinsed with a liquid CO_2 dryer and prior to imaging, the samples sputter coated.

4.10.2. Qualification of Differentiation

The scaffolds were fixed for 30 minutes at room temperature using 4% paraformaldehyde. After fixing, the scaffolds were rinsed 3 times with PBS. The scaffolds were permeabilized using 0.2% Triton x-100. The solutions used also included 1% BSA to remove the background of silk from staining. The scaffolds were left in the detergent for 45 minutes at room temperature. Afterwards, the scaffolds were rinsed with 5% BSA for 30 minutes at room temperature. The samples were then soaked in 250µL each of anti-mouse-e-cadherin primary antibody (1:100 dilution) overnight in 4°C. The next day, the samples were rinsed with 1X PBS 2-3 times. Following the rinse, the samples were soaked in 250µL of the anti-mouse-e-cadherin secondary antibody (1:250 dilution), 2X DAPI (1X dilution), and Alexa Fluor 488 Phalloidin green (1:30 dilution) for 1 hour at room temperature in foil. The samples were rinsed with 1X PBS 3 times and stored in 1X PBS. The scaffolds were scanned using a Leica SP2 confocal microscope. Scaffolds were observed using confocal microscopy and images were rendered in 3D using confocal software.

5. Results

5.1. Establishing Procedure for Making Featured Silk Hydrogels and Silk Sponges

The process for fabricating the 2D patterned scaffolds with villi only began with a wax mold. The features were machined using a CNC Milling Machine. Attached to the CNC Milling Machine, the bit used was a tapered ball end mill (Bits & Bits, TEB15-005). The tapered ball end mill was made of solid carbide with a cutting tip of .127mm, a length of cut of 10.16mm, and an included angle of 15 degrees. Following the milling, a carbide

pencil point tool was pressed into the features to make a sharper tip. The included angle was 15 degrees with a .0508mm tip. The blue wax mold was carved out according to the Solidworks design (Supplement A).

Following the machining of the master mold, a sequence of molds was used to acquire the final silk hydrogel scaffolds (Figure 12). Beginning with the wax mold, a release agent was used to aid in the removal of the material (Smooth-On Ease Release 200). Epoxy was casted into the wax mold (McMaster-Carr 7541A83). Following desiccation for 20 minutes, the epoxy was left to set overnight. Using the epoxy positive mold, we fabricated the negative using Sylgard 184 PDMS (Dow Corning Sylgard 184). The base wax mixed with the catalyst at a ratio of 10:1. The solution was poured into the epoxy mold and centrifuged at 5000rpm for 5 minutes. Then, the solution was left in a 60 degree incubator for 1 hour to cure. From the PDMS mold, a 5% w/v F-127 pluronic (Sigma Aldrich P2243) coating was applied for 10 minutes. Then the solution was removed and the pluronic was left to dry for 30 minutes. After applying the coating, the silk hydrogel was casted as previously indicated in section 4.2.

Due to issues with epoxy casting likely related to amine blush, the epoxy material was replaced with liquid rubber (Smooth-On Ecoflex 00-35). In addition, due to issues of compatibility between materials, the Sylgard material was also replaced with the liquid rubber. The resulting process ended up using a series of molds with the following materials: wax, rubber, rubber, silk hydrogel.

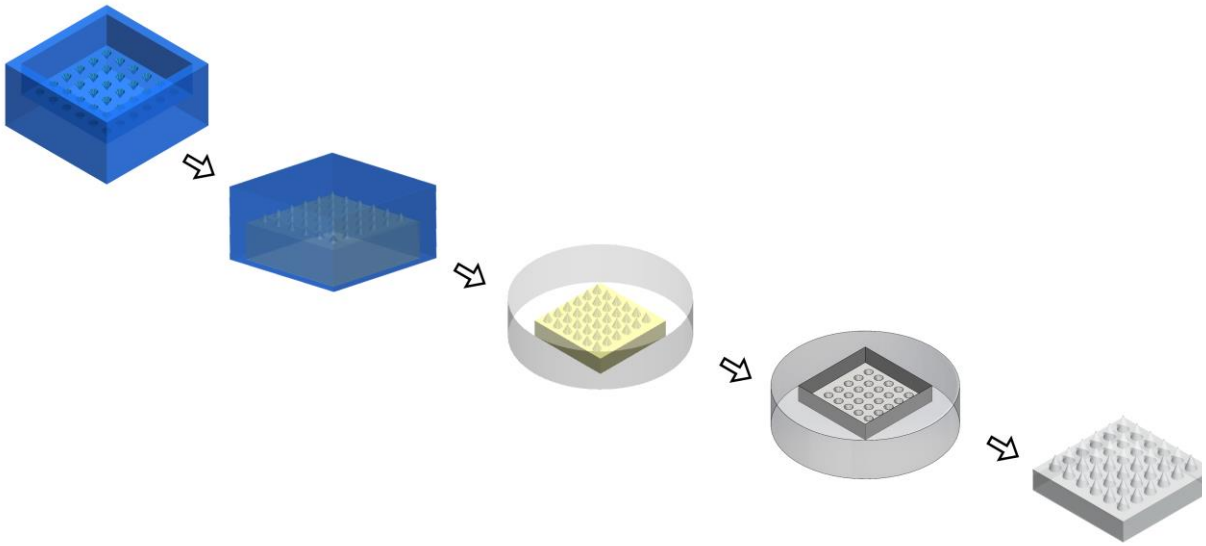

Figure 12. Mold Making Schematic for Villi Only from Wax Molds. The process involved a series of molds made with the following materials: wax, epoxy, PDMS, silk hydrogel. Afterwards, the process was modified to use the following materials: wax, rubber, rubber, silk hydrogel.

5.2. 3D Printing Method for Villi and Crypts (Positive and Negative Masters)

The process for fabricating the 2D patterned scaffolds with villi and crypts began with a 3D printed resin mold. The molds were printed using the Form2 SLA 3D Printer. Initially, the molds were printed using black resin. With a desire to see the features more easily under an optical microscope, the material used for printing was a clear resin. The resin molds were printed according to the Solidworks designs (Supplements B-G).

With concerns for high enough resolution printing, negative and positive master molds were printed. The process was similar to Figure 12 when using the negative master mold.

Rather than beginning with a machined wax mold, the process of fabrication began with a printed resin mold.

With a positive master mold, the process was simplified (Figure 13). Beginning with a 3D printed resin mold, a release agent was used to aid the removal of the material (Smooth-On Ease Release 200). Liquid rubber was casted onto the 3D printed mold, centrifuged at 4000rpm for 5 minutes, and left to cure. Following curing, the pluronic coating could be applied and the silk hydrogels could be formulated as indicated in section 5.1.

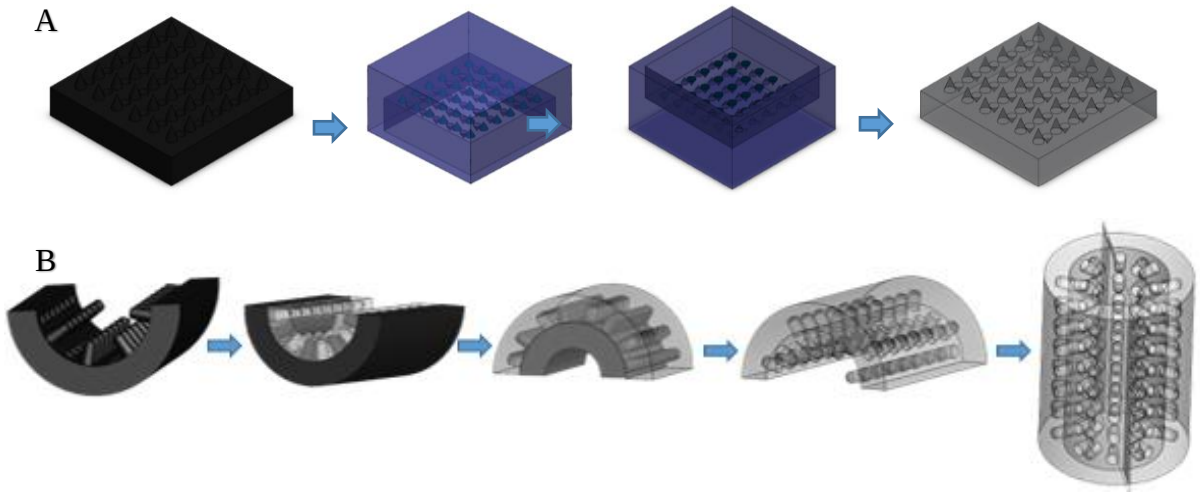

Figure 13. Mold Making Schematic for Scaffolds from Positive 3D Printed Molds. A) Flat, 2D Molds. The process involved a series of molds made with the following materials: resin, rubber, silk hydrogel. Various liquid rubbers and Sylgard 184 PDMS was tested to be a part of the fabrication process. B) 3D Molds. The process was similar to the flat molds. The only difference was that a half cylindrical geometry was fabricated at first and combined at the end to form a cylindrical shape.

5.3. 3D Printed Molds and Sequential Molds

In order to create the scaffolds, various molds were fabricated. We used 2 different methods of fabrication to obtain villi and crypts features on the final scaffolds. The first method involved the use of micromachining on a wax block, which could fabricate villi features only. The second method involved the use of SLA printing from the Form2 Printer on a resin mold.

5.3.1. Series of Molds Used in Fabrication from Wax Molds

The first method of fabrication of the silk hydrogels consisted of 4 main molds: wax block (Figure 14), epoxy (Figure 15), Sylgard 184 silicone elastomer or PDMS (figure 16), and silk hydrogel (Figure 17). This was the original method of fabrication being used to make the patterned silk hydrogels. We originally considered making the silk hydrogels directly from the wax molds. However, there was the issue of reproducibility. The silk hydrogel material did not separate from the mold easily, resulting in lost features and material left behind on the mold. As the epoxy material came off most easily from the wax mold and the silk hydrogel material came off most easily from the Sylgard silicone material, the four step process was used with the wax mold. In terms of greater production as well, it is more efficient and cheaper to produce PDMS for the making of the featured silk hydrogels than to machine wax molds constantly. In addition, throughout the fabrication process, we came across the issue of the features not being replicated well. This was likely due to the viscosity of the molding solutions. There was a need to determine the best rotation speed and time for centrifugation to pull the solution into the features of the mold, which resulted in the established methods previously indicated.

A

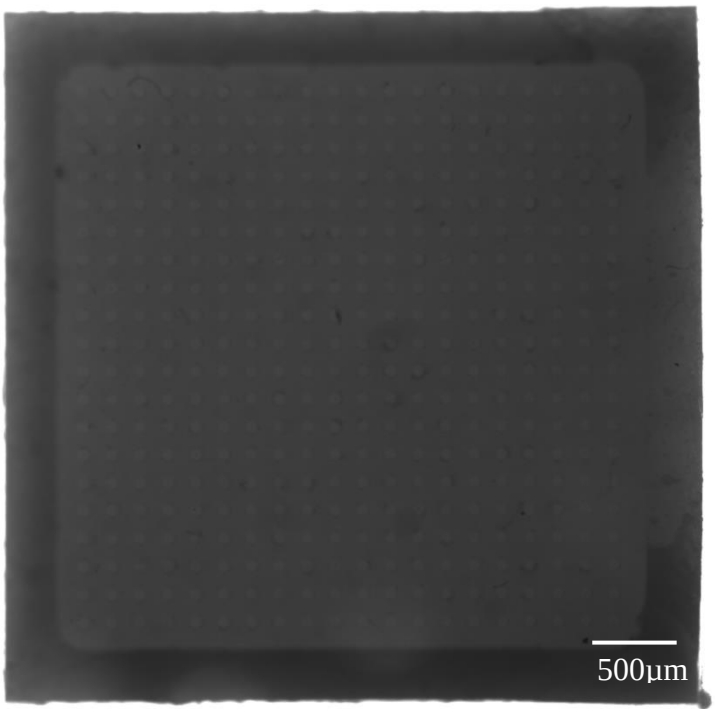

B

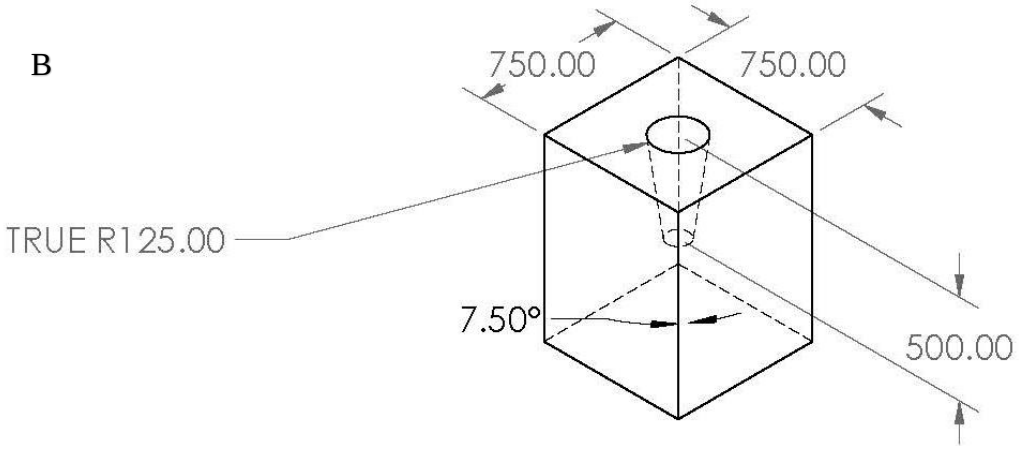

Figure 14. First Mold in Wax Sequence. A) Wax block. Brightfield microscopy. A tapered ball end mill was used. It had a 15 degree tilt with a .004" diameter ball end. The resulting wax mold had 20 by 20 villi features, shaped like cylindrical cones. The cylindrical cones had approximately 125µm diameter and 500µm depth with a 7.5 degree side angle. B) An example of what one of the features looked like in the wax mold.

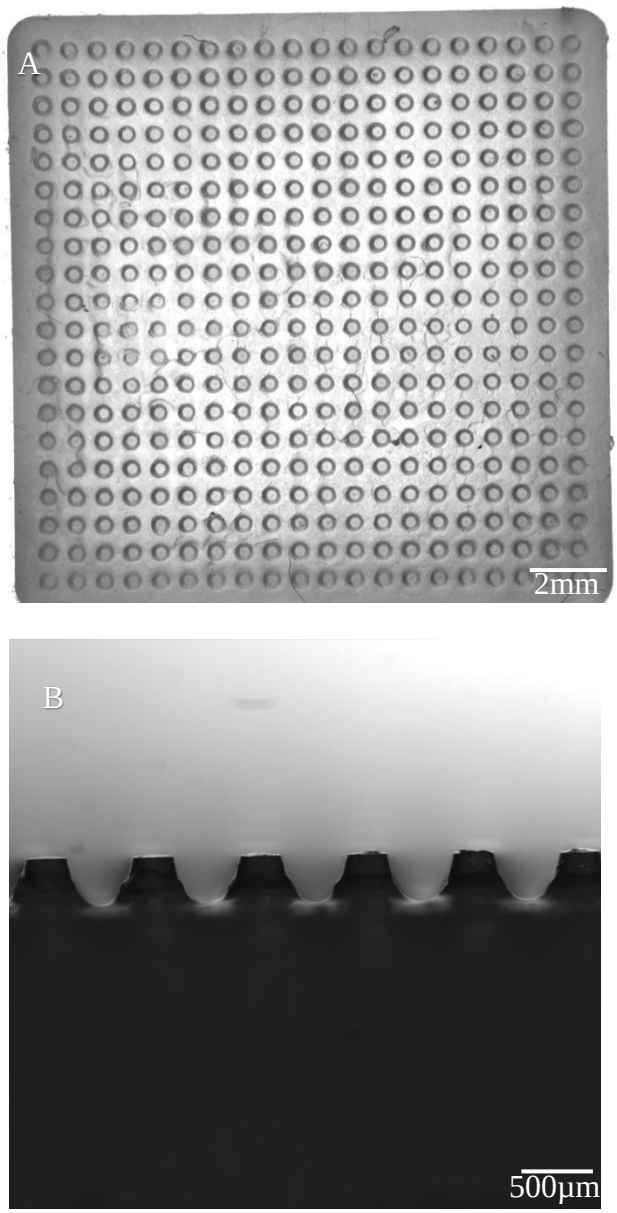

Figure 15. Second Mold in Wax Sequence. The epoxy solution was poured into the cutout of the wax block, centrifuged, and allowed to harden for 24 hours in room temperature. A) Top view of the epoxy mold. Brightfield microscopy. The material was made from epoxy structural adhesives. The resulting mold was positive. B) Side view of the epoxy mold. Brightfield microscopy. The presence of villi can be seen in this mold with a shape similar to what was expected.

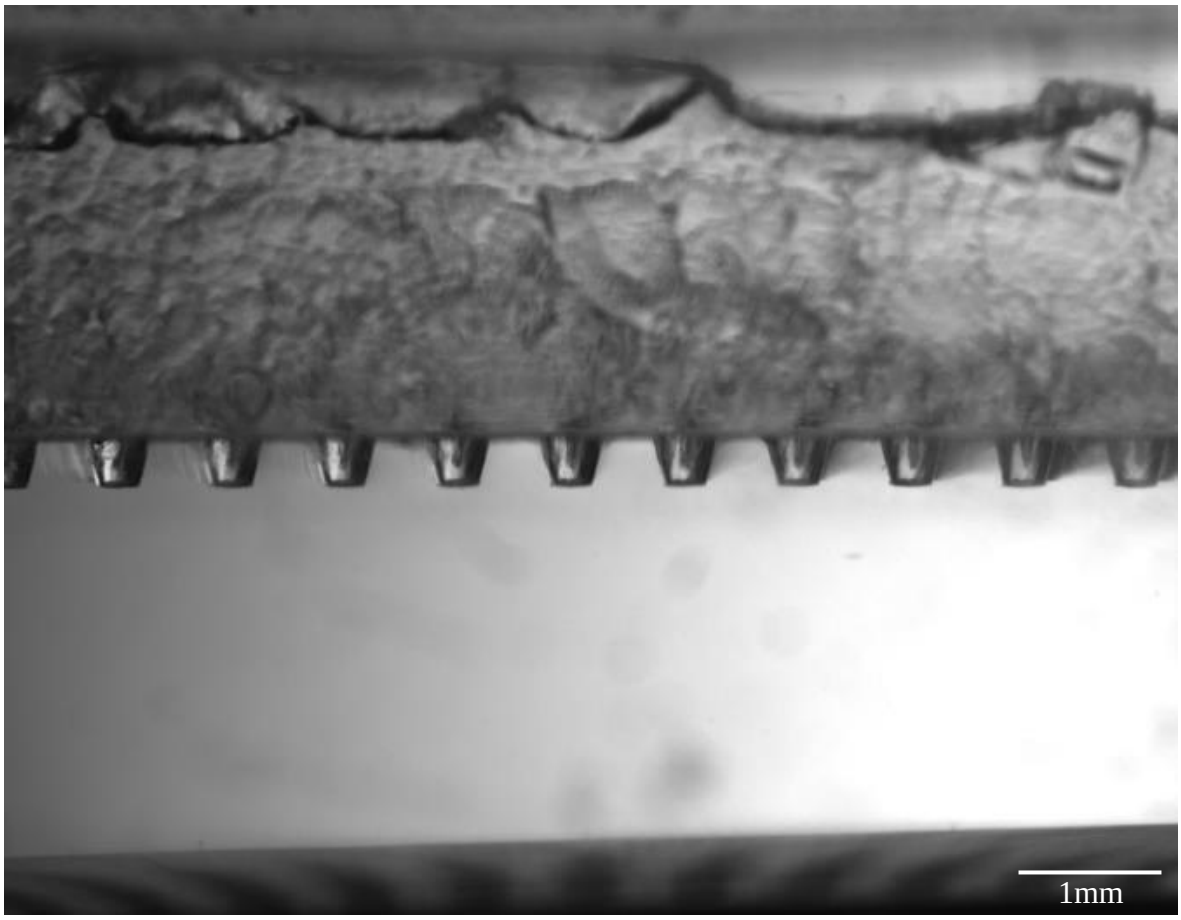

Figure 16. Third Mold in Wax Sequence. Brightfield microscopy. The epoxy mold was taped to the bottom of a petri dish. Afterwards, the Sylgard 184 silicone elastomer solution was mixed and poured into the dish. The result was the imprint of the epoxy mold in the Sylgard 184 silicone.

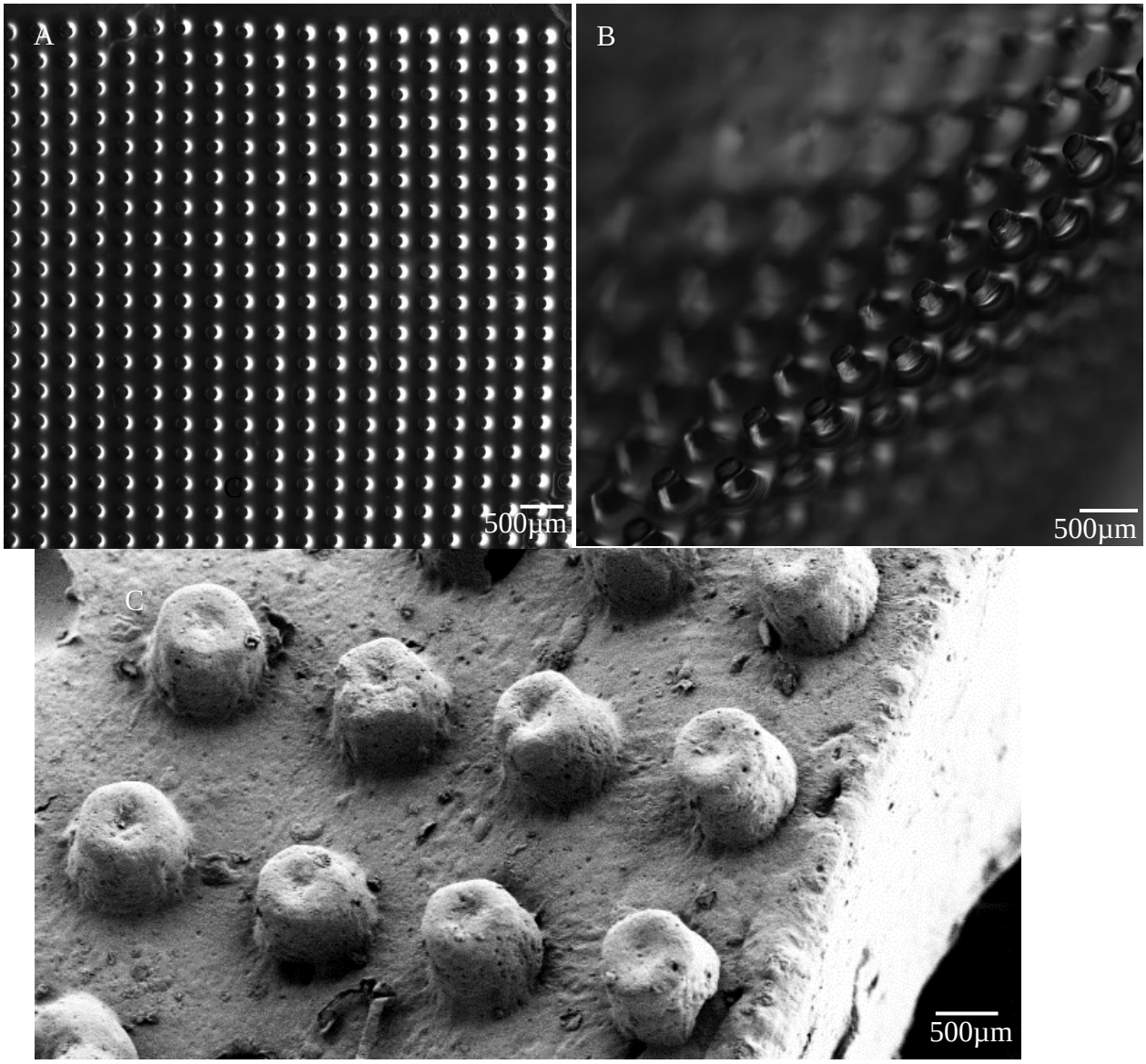

Figure 17. Final Silk Hydrogel Scaffold in Wax Sequence. The silk hydrogel solution was mixed and poured into the imprint left from the epoxy mold in the Sylgard 184 silicone. The result was the positive image of the scaffold. A) Top view of the silk hydrogel scaffold. Brightfield microscopy. B) Side view of the silk hydrogel scaffold. Brightfield microscopy. C) SEM image of the silk hydrogels. The patterned villi features was seen and replicated from the original mold.

5.3.2. Fabrication of the Silk Hydrogels and Sponges from the Flat Resin Molds

5.3.2.1. 500µm Villi, 300µm Crypts, 300µm Diameter Positive Resin Molds

The second method of fabrication of the silk hydrogels consisted of 3 main molds: resin (Figure 18), Ecoflex 00-35 rubber (Figure 19), and silk hydrogel (Figure 20). This was the initial attempt of printing the design of 300µm diameter with 500µm height villi and 300µm depth crypts.

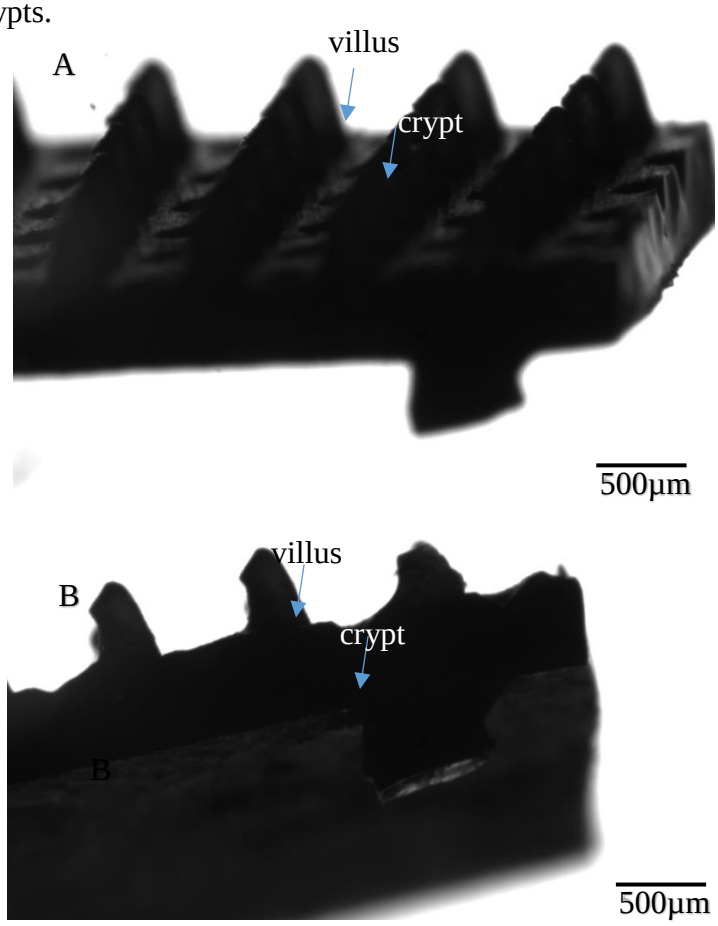

Figure 18. 500µm Villi, 300µm Crypts, 300µm Diameter Resin Mold. This was the first mold in the sequence, the positive resin mold. A) Positive resin mold. Brightfield microscopy. The resulting resin mold had features with 600µm spacing between the centers of each feature. The design consisted of 500µm height villi and 300µm depth crypts with 300µm diameter and a 4 degree side angle for each feature. B) Another side view of resin mold. Brightfield microscopy. The depth of the crypts was around 30µm. The height of the villi was around 500µm. The images were labeled with what the features replicated on the final scaffolds.

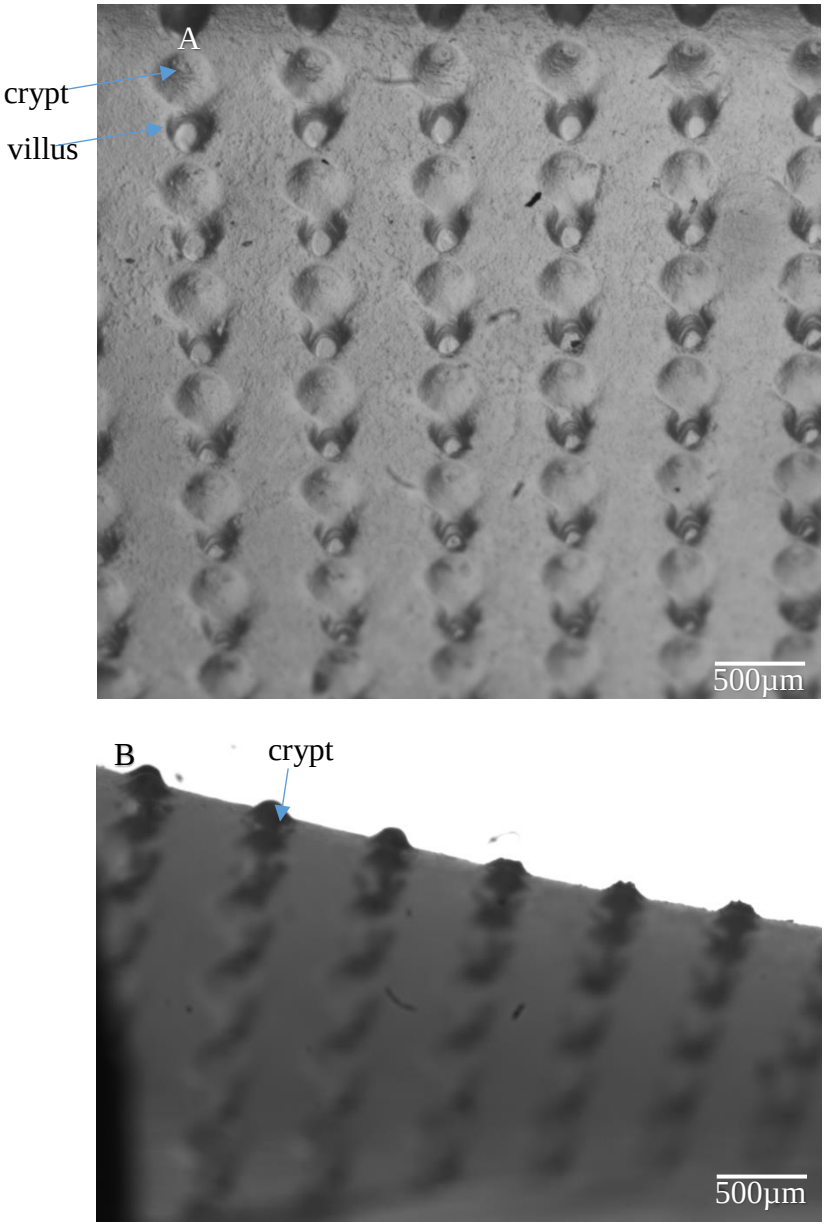

Figure 19. 500µm Villi, 300µm Crypts, 300µm Diameter Ecoflex 00-35 Rubber Mold. This was the second mold in the sequence, the negative rubber mold. A) Top view of the rubber mold. Brightfield microscopy. The resulting mold was the negative image of the final scaffold with 600µm spacing between the centers of each feature. B) Side view of the rubber mold. Brightfield microscopy. The presence of crypts was seen in this mold with a conical shape approximately 30µm tall. The images were labeled with what the features replicated on the final scaffolds.

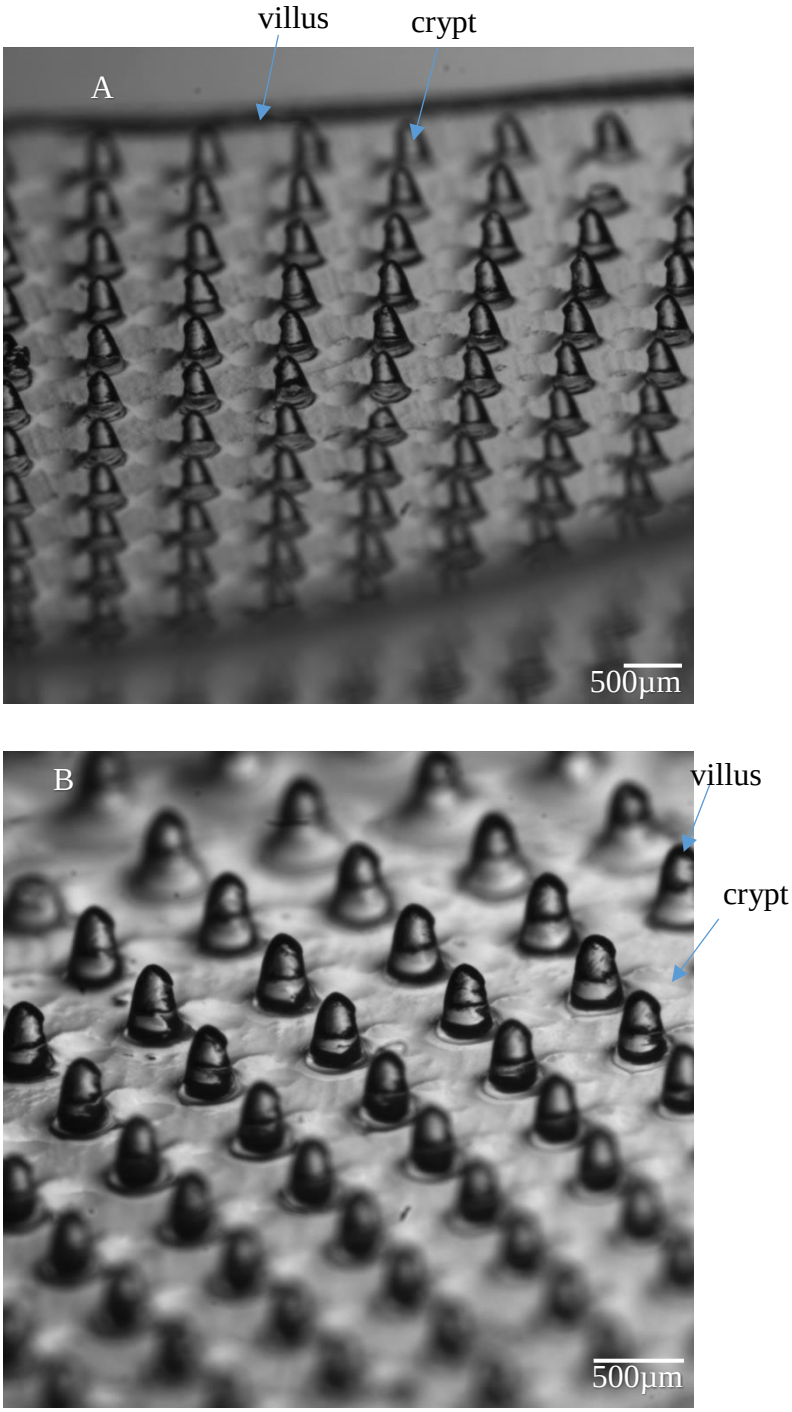

Figure 20. 500µm Villi, 300µm Crypts, 300µm Diameter Silk Hydrogel. This was the final part of the sequence, the silk hydrogel scaffold. A) Top view of the silk hydrogel scaffold. Brightfield microscopy. The resulting scaffold had features with 600µm spacing between the centers of each feature. The diameter of the features are approximately 300µm. B) Side view of the silk hydrogel scaffold. Brightfield microscopy. The patterned villi crypts features were seen and replicated from the original mold. The villi were shaped like a cone and approximately 500µm tall. The images were labeled with what the features replicated on the final scaffolds.

5.3.2.2. 800µm Villi, 700µm Crypts, 500µm Diameter Positive Resin Molds

The second method of fabrication of the silk hydrogels consisted of 3 main molds: resin, Ecoflex 00-35 rubber, and silk hydrogel (Figure 21). The molds were also used to create film-coated silk sponges (Figure 22). The silk hydrogel (Figure 23) and silk sponge scaffolds (Figure 24) were also capable of having walls. The mold was designed to have 800µm villi and 700µm crypts shaped as cones with 500µm diameter.

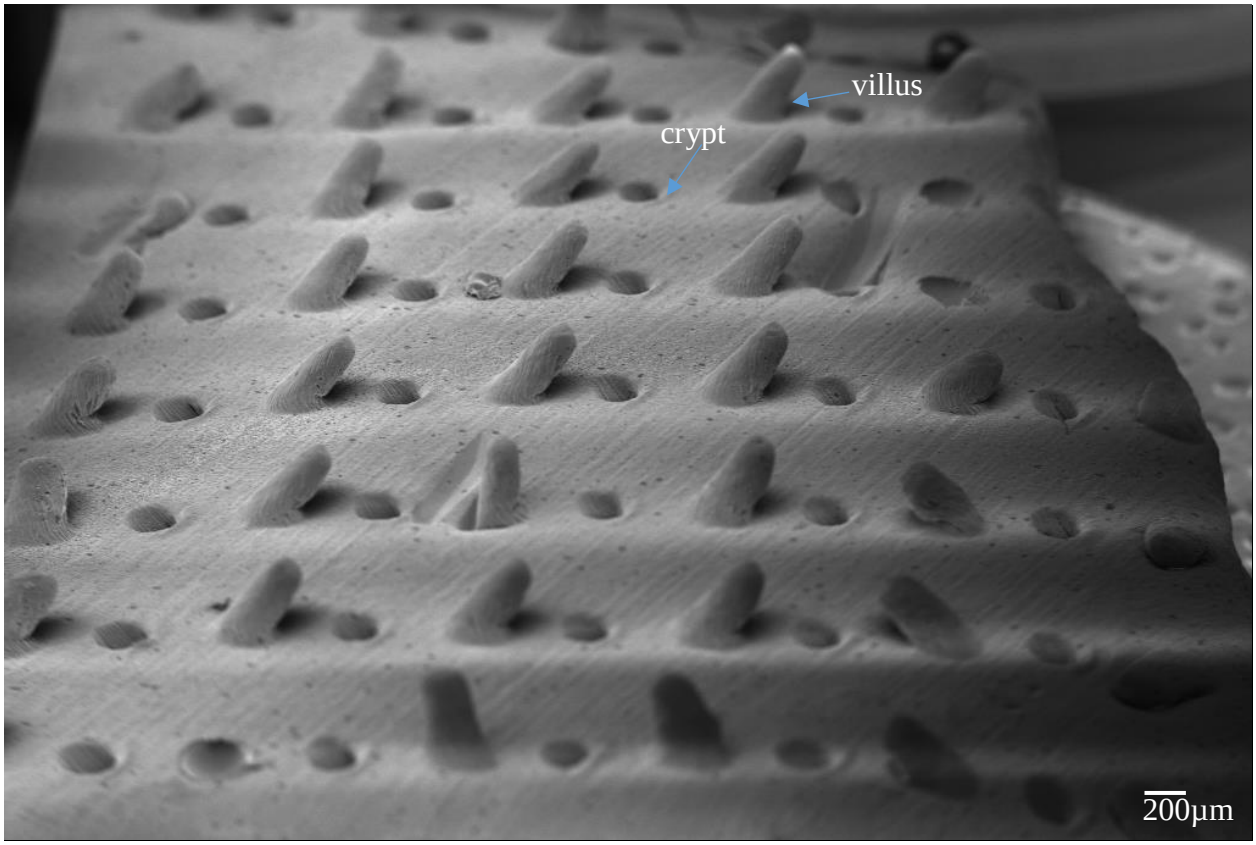

Figure 21. 800µm Villi, 700µm Crypts, 500µm Diameter Silk Hydrogel. This was the final part of the sequence, the silk hydrogel scaffold. A) Top view of silk hydrogel. Brightfield microscopy. The villi were approximately 800µm with 500µm diameter. B) Side view of the silk hydrogel. SEM. The villi were slightly tilted and the diameter of the crypts was 500µm. The pattern of the original resin material was seen on the final silk hydrogel. The patterned villi crypts features were seen and replicated from the original mold. The images were labeled with what the features replicated on the final scaffolds.

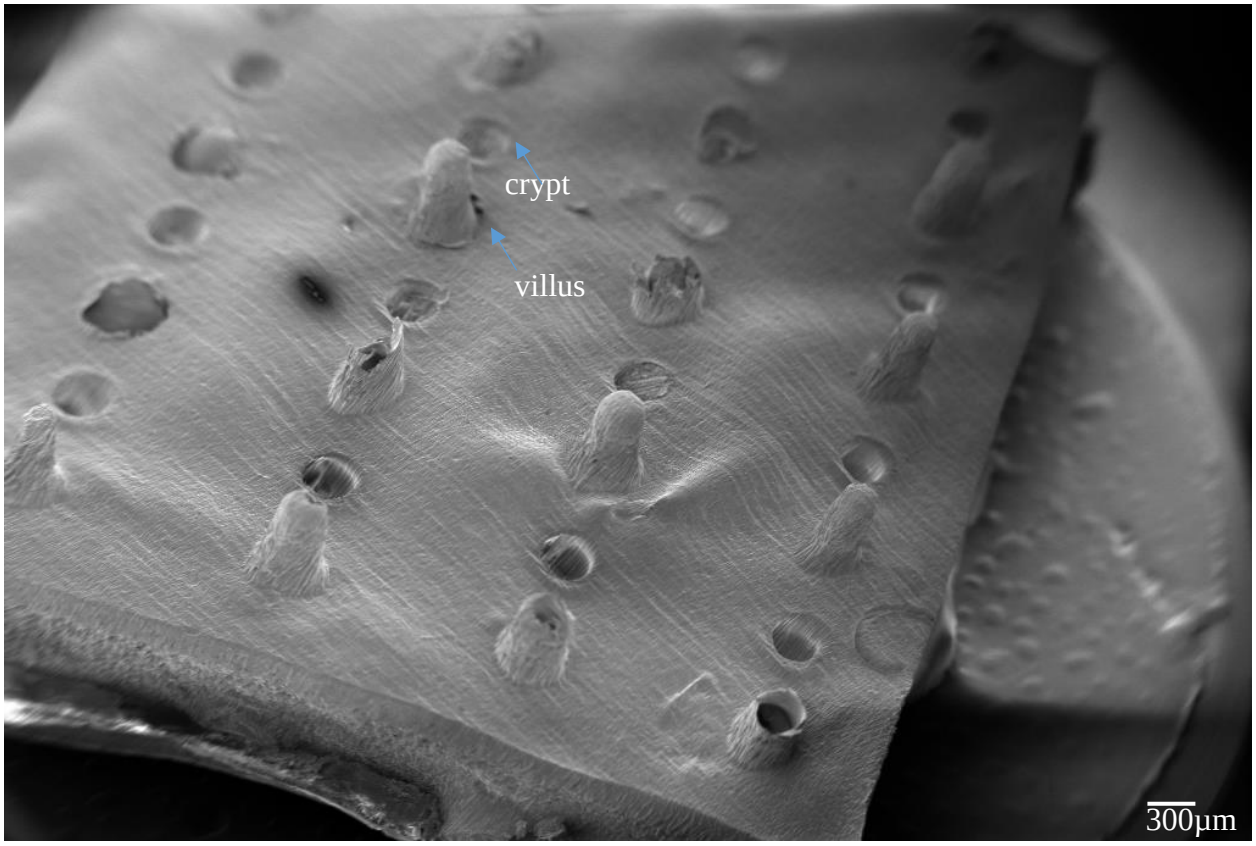

Figure 22. 800µm Villi, 700µm Crypts, 500µm Diameter Film-Coated Silk Sponges. Using the same rubber mold, a film coated silk sponge scaffold was also made. A) Top view of the sponge scaffold. SEM. The patterned villi and crypts features were seen and replicated from the original mold. The pores were also minimized by the film coating. B) Side view of the sponge scaffold. Brightfield microscopy. The villi were approximately 300µm, indicating that the features may have not been fully replicated or that they shrunk. The images were labeled with what the features replicated on the final scaffolds.

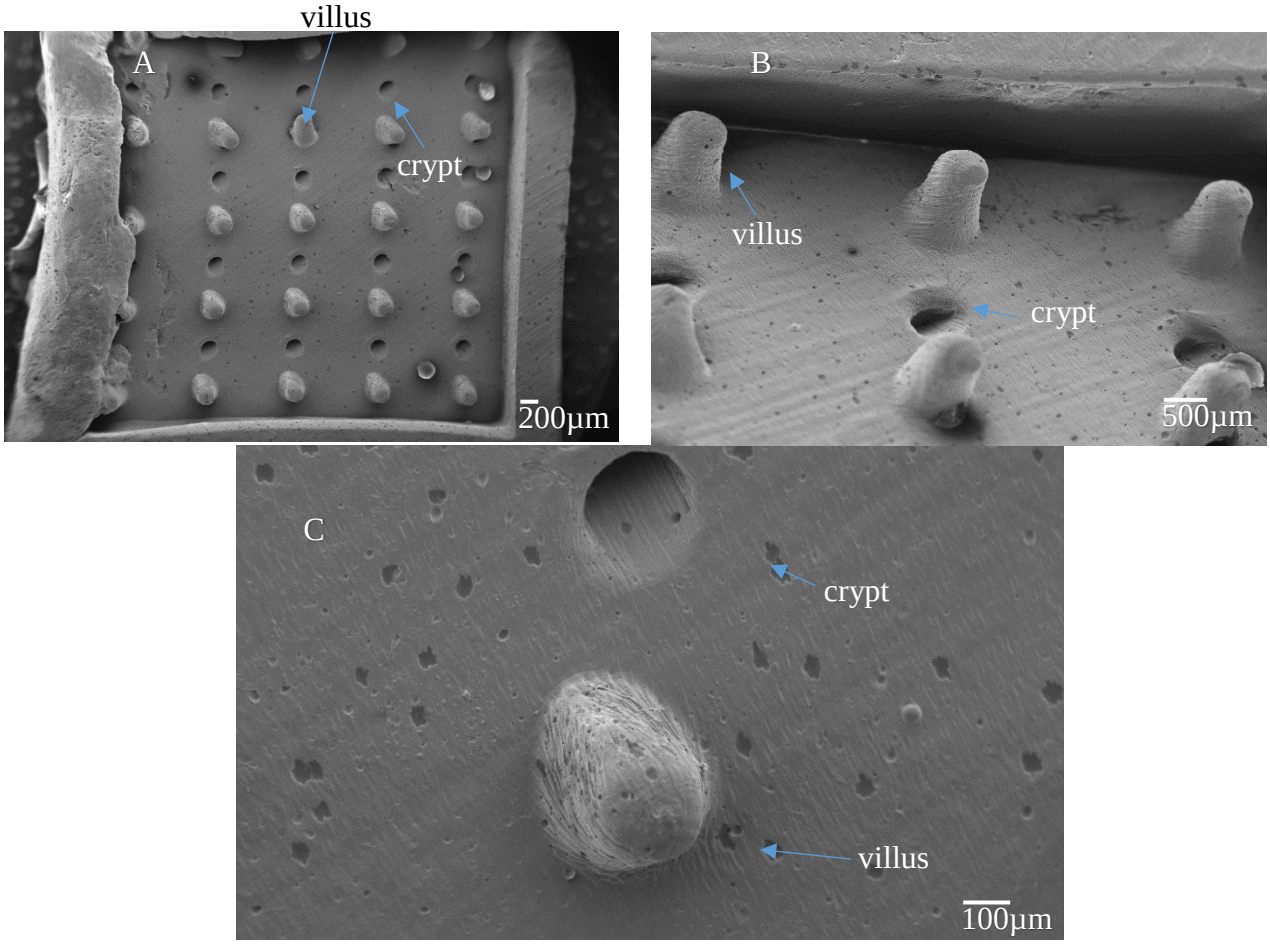

Figure 23. 800µm Villi, 700µm Crypts, 500µm Diameter Silk Hydrogels with Walls. Using the same sequence of molds, beginning with a positive resin mold, silk hydrogel scaffolds with walls were created. The pieces were approximately 1mm by 1mm. A) Top view of hydrogel with walls. SEM. The features had a consistent shape and size with 1000µm spacing between the centers of each feature. B) Side view of the hydrogel with walls. SEM. The villi had a slight tilt at the tips and were approximately 800µm. C) Close up of top of features. The diameter of the features were 500µm. The crypts had a tilted conical shape. The images were labeled with what the features replicated on the final scaffolds.

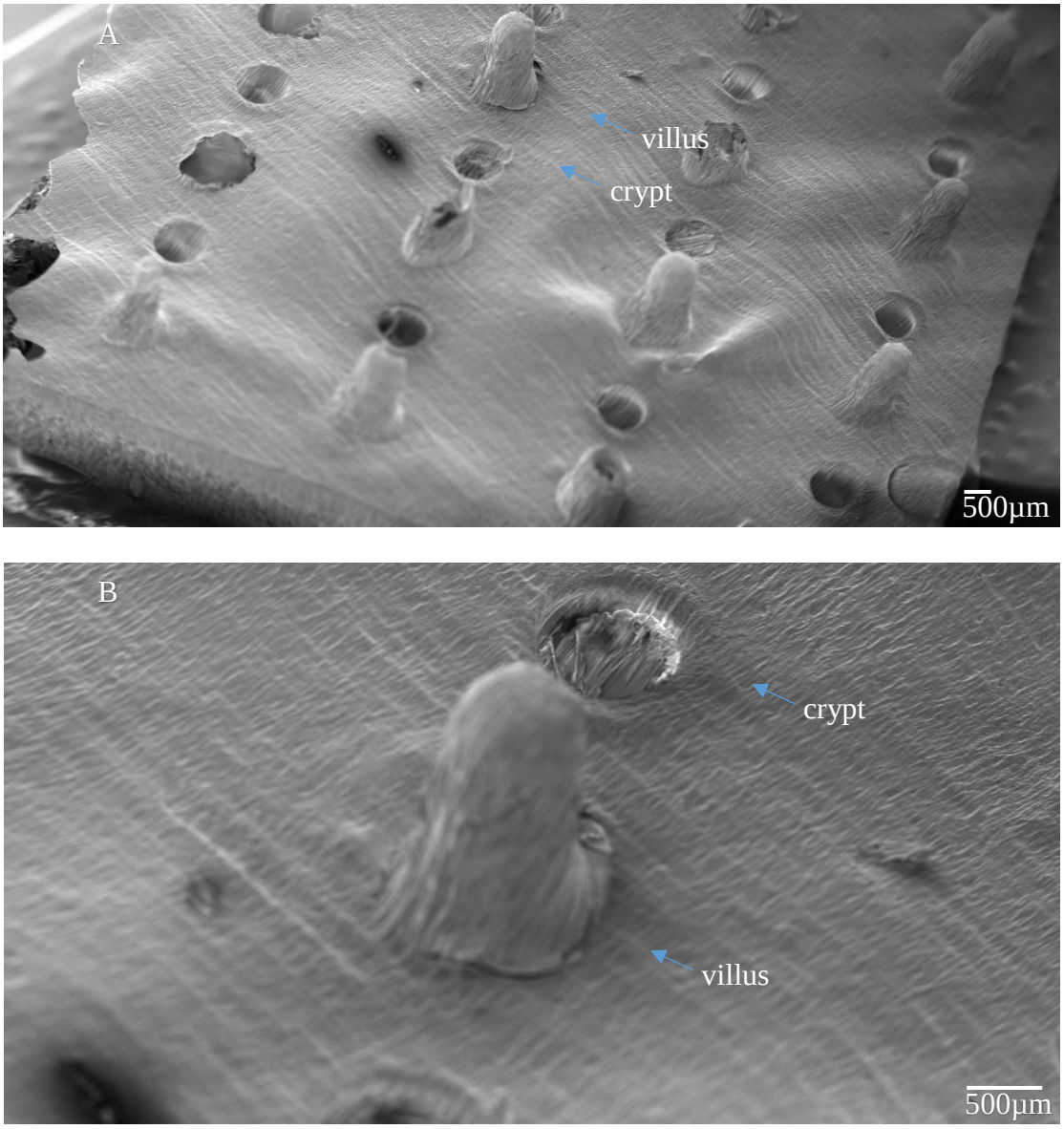

Figure 24. 800µm Villi, 700µm Crypts, 500µm Diameter Silk Sponges with Walls. Using the same sequence of molds, beginning with a positive resin mold, silk sponge scaffolds with walls were created. The pieces were approximately 1mm by 1mm. A) Top view of sponge with walls. SEM. The features were consistent, although some features appeared to be ripped. B) Close up side view of villus and crypt. SEM. The diameters were about 500µm. The villus were approximately 800µm. The crypts had a tilted conical shape. The images were labeled with what the features replicated on the final scaffolds.

5.3.2.3. 800µm Villi, 700µm Crypts, 500µm Diameter Negative Resin Molds

This method of fabrication of the silk sponge consisted of 2 main molds: resin (Figure 25) and silk sponge (Figure 26). The mold was designed to have 800µm villi and 700µm crypts shaped as cones with 500µm diameter and a 4 degree side angle.

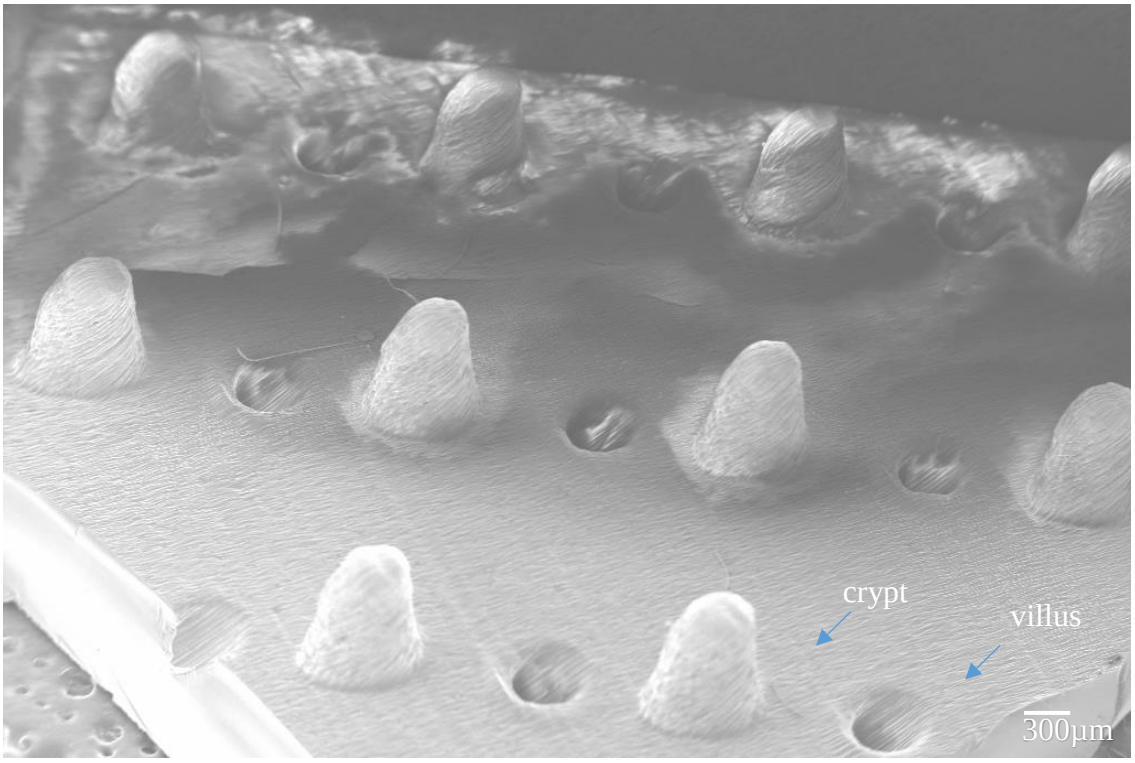

Figure 25. 800µm Villi, 700µm Crypts, 500µm Diameter Negative Resin Mold. SEM. This was the first mold in the sequence, the negative resin mold. The resulting resin mold had features with 1000µm spacing between the centers of each feature. The design consisted of 800µm height villi and 700µm depth crypts with 500µm diameter and a 4 degree side angle for each feature. The peaks formed the crypts. The wells formed the villi. The crypts were a cylindrical shape with a 500µm diameter and 700µm height. The villi had the same diameter but appeared to have a tilted cylindrical shape. The images were labeled with what the features replicated on the final scaffolds.

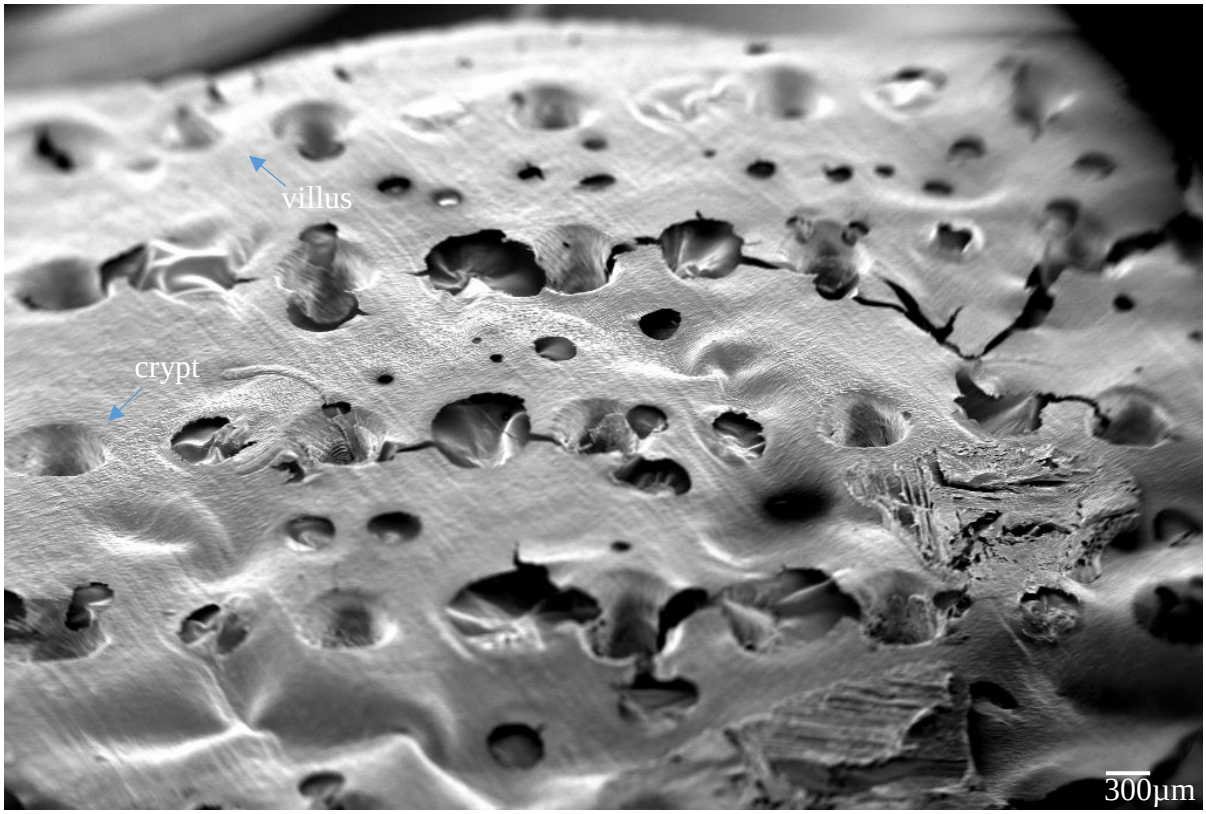

Figure 26. 800µm Villi, 700µm Crypts, 500µm Diameter Silk Sponges from Negative Resin Mold. SEM. This was the final part of the sequence, the film-coated silk sponge. This was the top view of the scaffold. The villi were not consistent. The villi that did form from the mold had a tilt that distorted the shape. The diameter of the features were approximately 500µm. The images were labeled with what the features replicated on the final scaffolds.

5.3.3. Fabrication of the Silk Hydrogels and Sponges from the 3D Resin Molds

5.3.3.1. 800µm Villi, 700µm Crypts, 500µm Diameter Positive Half Cylinder Molds

The method of fabrication of the 3D silk hydrogels consisted of 3 main molds: resin, Ecoflex 00-35 rubber, and silk hydrogel (Figure 27). 3D silk sponges were also made using the same method (Figure 28). The mold was designed to have 800µm villi and 700µm crypts shaped as cones with 500µm diameter and a 4 degree side angle.

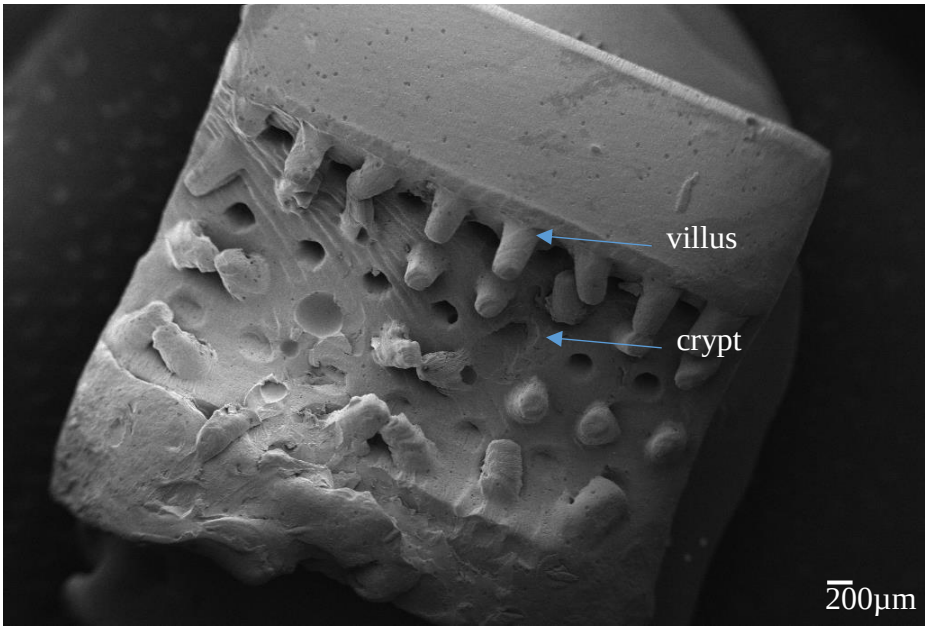

Figure 27. 800µm Villi, 700µm Crypts, 500µm Diameter Positive Half Cylinder Hydrogel. This was the final part of the sequence, the silk hydrogel scaffold. Top view of half cylinder hydrogel. SEM. The features were consistent and evenly spaced. The diameter of the features were around 400µm. The 3D hollow half cylindrical shape was replicated on the final scaffold. The villi were around 800µm with a cylindrical cone shape. The crypts appeared to have a slight tilt as indicated by the depth. The patterned villi crypts features were seen and replicated from the original mold. The images were labeled with what the features replicated on the final scaffolds.

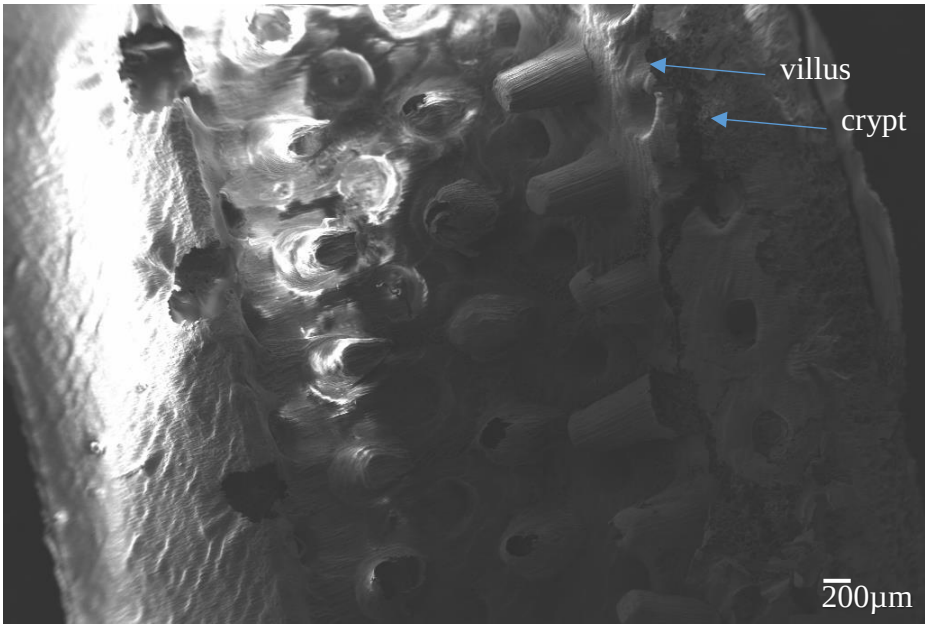

Figure 28. 800µm Villi, 700µm Crypts, 500µm Diameter Positive Half Cylinder Film-Coated Silk Sponge. Using the same rubber mold, a film coated silk sponge scaffold was also fabricated. Top view of half cylinder sponge. SEM. The features were consistent and evenly spaced. The diameter of the features were around 400µm. The 3D hollow half cylindrical shape was replicated on the final scaffold. The villi were around 800µm with a cylindrical cone shape. The crypts appeared to have a slight tilt as indicated by the depth. The patterned villi crypts features were seen and replicated from the original mold. The images were labeled with what the features replicated on the final scaffolds.

5.3.3.2. 800µm Villi, 700µm Crypts, 500µm Diameter Negative Half Cylinder Molds

This method of fabrication of the silk hydrogels consisted of 2 main molds: resin (Figure 29), silk sponge (Figure 30). The original resin mold had 800µm wells and 700µm protrusions. The mold was designed to have 800µm villi and 700µm crypts shaped as cones with 500µm diameter and a 4 degree side angle.

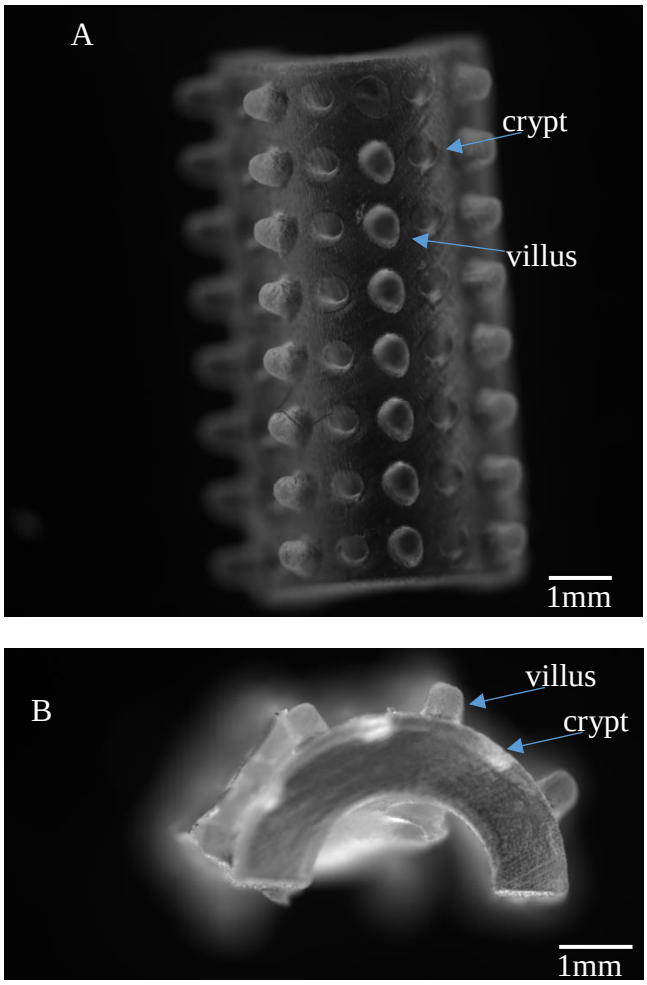

Figure 29. 800µm Villi, 700µm Crypts, 500µm Diameter Negative Half Cylinder Resin Mold. This was the first mold in the sequence, the negative resin mold. A) Top view of positive half cylinder resin mold. Brightfield microscopy. The resulting resin mold had features with 1000µm spacing between the centers of each feature. The diameter of the features was approximately 500µm. B) Side view of half cylinder resin mold. Brightfield microscopy. The height of the protrusion was around 700µm. The images were labeled with what the features replicated on the final scaffolds.

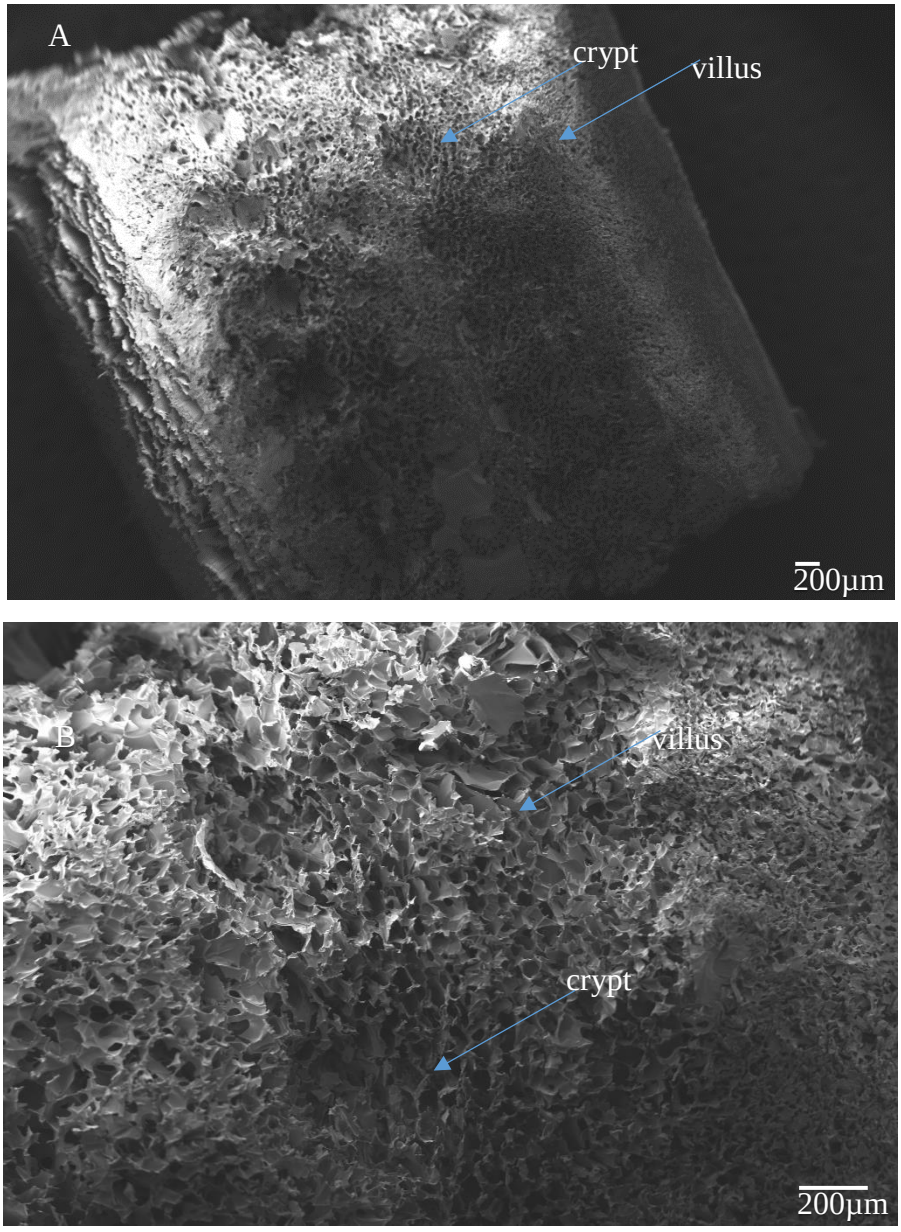

Figure 30. 800µm Villi, 700µm Crypts, 500µm Diameter Negative Half Cylinder Silk Sponge. This was the final part of the sequence, the silk sponge scaffold. A) Top view of the silk sponge scaffold. The patterned villi and crypts features were smaller than expected. B) Close up view of the silk sponge scaffold. The crypts were shallow in depth and the villi were smaller than expected in diameter and height. The film coating was not present on the final scaffold. The images were labeled with what the features replicated on the final scaffolds.

5.3.4. Pore Size of Silk Sponge, Silk Hydrogel, and Film-Coated Silk Sponge

In order to recreate the effect of renewal, the cells must be capable of adhering to the surface and proliferating from the crypts up to the villi. The materials used for the intestinal scaffold should have pore sizes smaller than the average cell. The following materials were considered for the scaffold: silk sponge (Figure 31), silk hydrogel (Figure 32), and film-coated silk sponge (Figure 33).

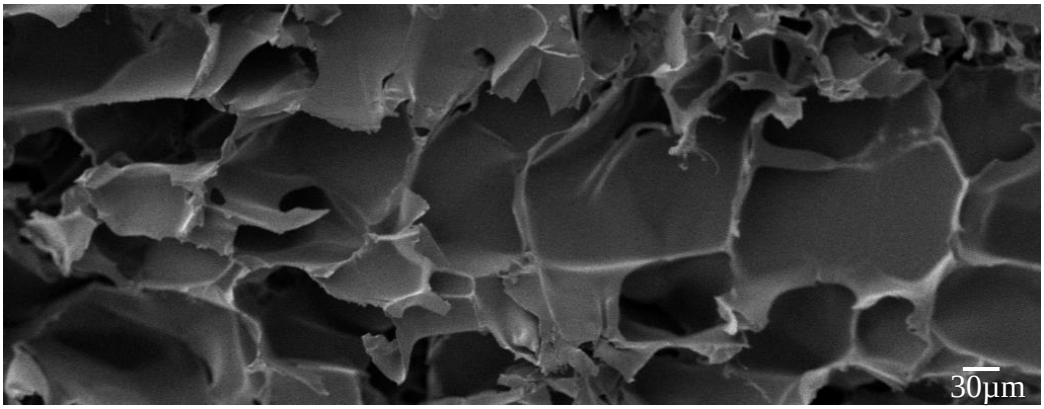

Figure 31. Silk Sponge Pores. SEM image. The pore sizes were relatively large and ranged from approximately 30µm to 150µm.

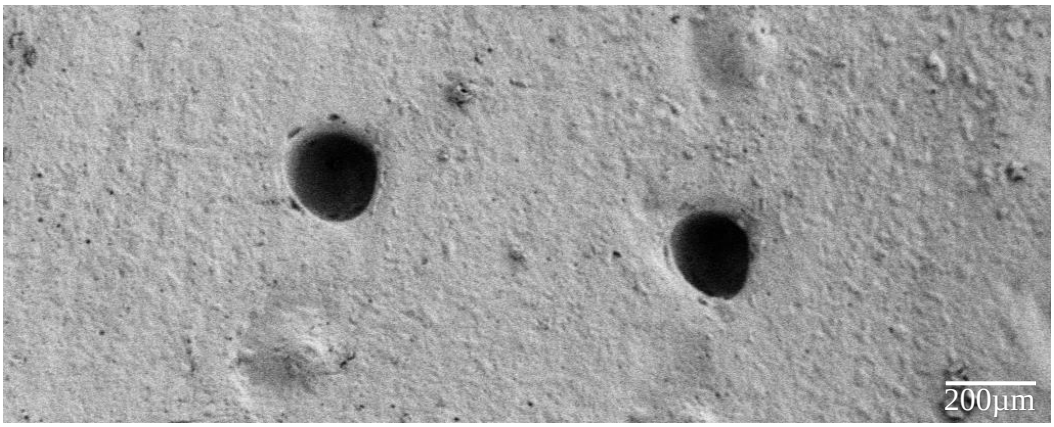

Figure 32. Silk Hydrogel Pores. This was a silk hydrogel with 300µm holes and 50µm protrusions. This came from the resin mold that was designed to have 300µm diameter features with 300µm crypts and 500µm villi. As seen in the image, the pore sizes were very small.

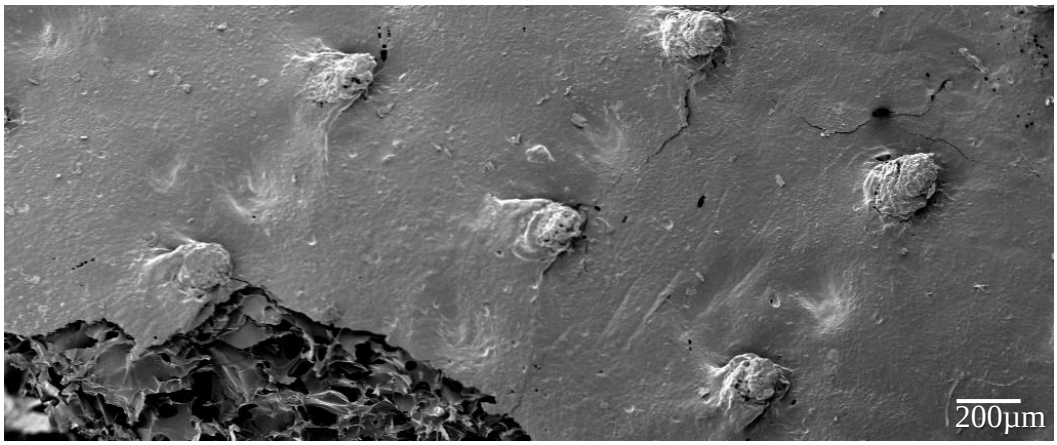

Figure 33. Film-Coated Silk Sponge Pores. This scaffold came from the resin mold that was designed to have 500µm diameter with 700µm crypts and 800µm villi. The silk sponge material was seen underneath the silk film coating. The film coating minimized the pore sizes on the surface of the silk sponge, creating a similar surface to the silk hydrogels.

5.4. Caco-2 Cells and Enteroids Seeded on Silk Hydrogel Scaffolds

5.4.1. Caco-2 Cells Seeded on Silk Hydrogel Scaffolds with Villi

Initially, Caco-2 cells were seeded on silk hydrogel scaffolds in order to determine the best concentration for intestinal cell adherence to silk hydrogels. Caco-2 cells were able to cover the villi of the silk hydrogel scaffold using 50ug/cm^2 collagen type I coating (Figure 34).

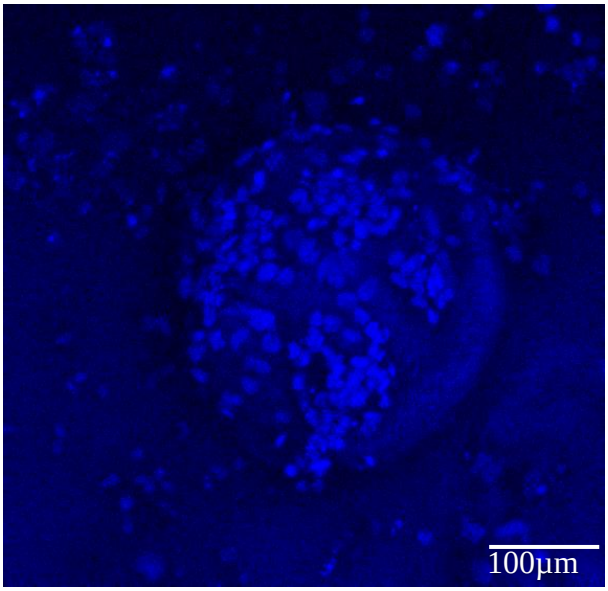

Figure 34. Caco-2 Cells on Silk Hydrogel. Keyence microscope. DAPI staining (blue) was used. Caco-2 cells were seeded on silk hydrogel scaffolds with 500µm villi made from the wax blocks. The Caco-2 cells were capable of covering the villi on the silk scaffolds.

5.4.2. Enteroids Seeded on Silk Hydrogel Scaffolds with Villi and Crypts

Human intestinal stem cell-derived ileum enteroids were seeded on collagen-coated silk hydrogel scaffolds with villi and crypts. 50ug/cm^2 collagen type I coating was used. Approximately 1 well (of a 24 well plate used to expand enteroids) was seeded per scaffold. After 7 days of proliferation and 5 days in differentiation medium, there was full coverage of the villi features (Figure 35). The cross section of a single villus showed the cell polarization (Figure 36).

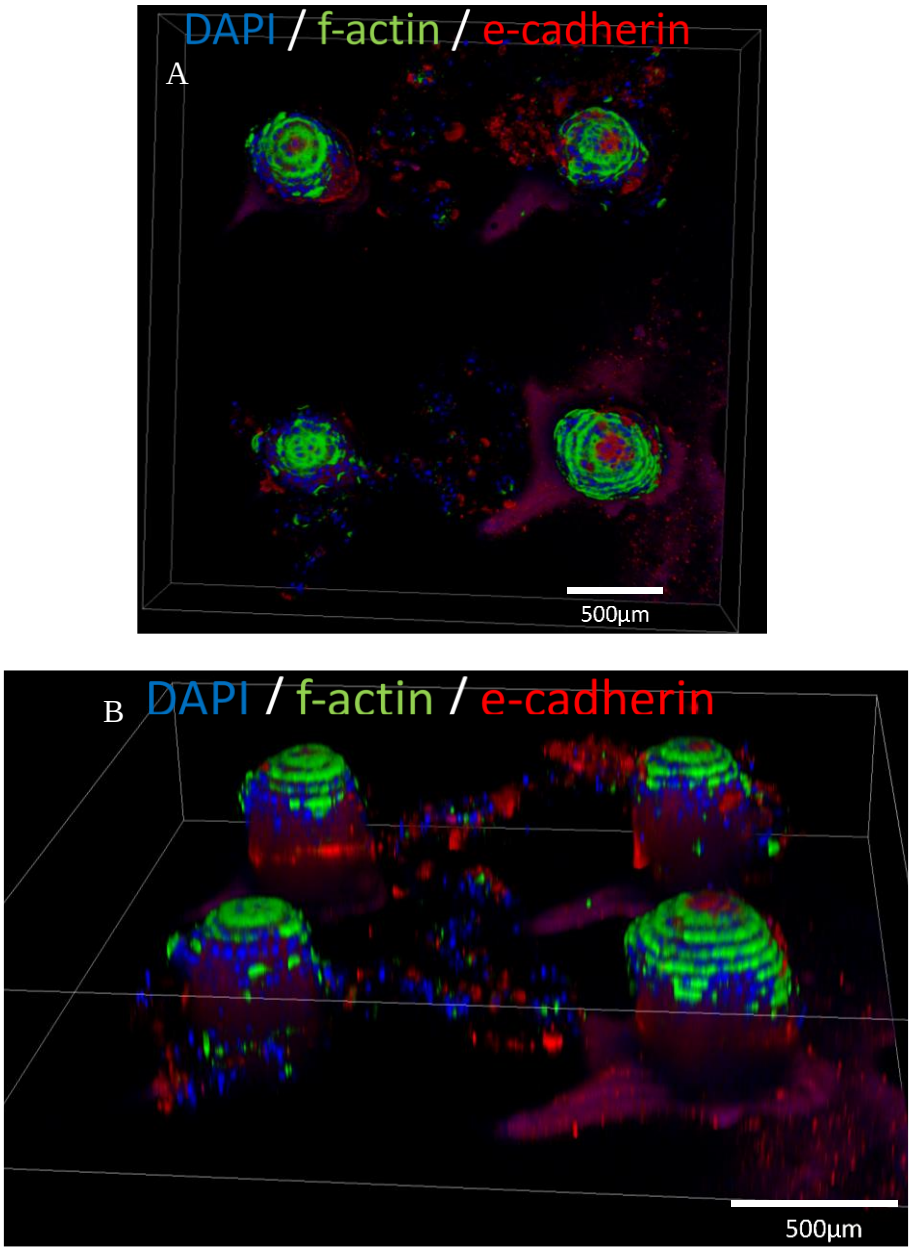

Figure 35. Silk Hydrogel with Villi Covered by Enteroids. Confocal microscopy. The tips of the silk hydrogel scaffolds, coated with collagen type I, were seeded with ileum enteroids. These images were acquired using DAPI (blue), f-actin (green), and e-cadherin (red) staining. A) Top view. B) Side view. Cell nuclei was seen throughout the features. There were rings of actin and cells with tight junction formation on each villus feature.

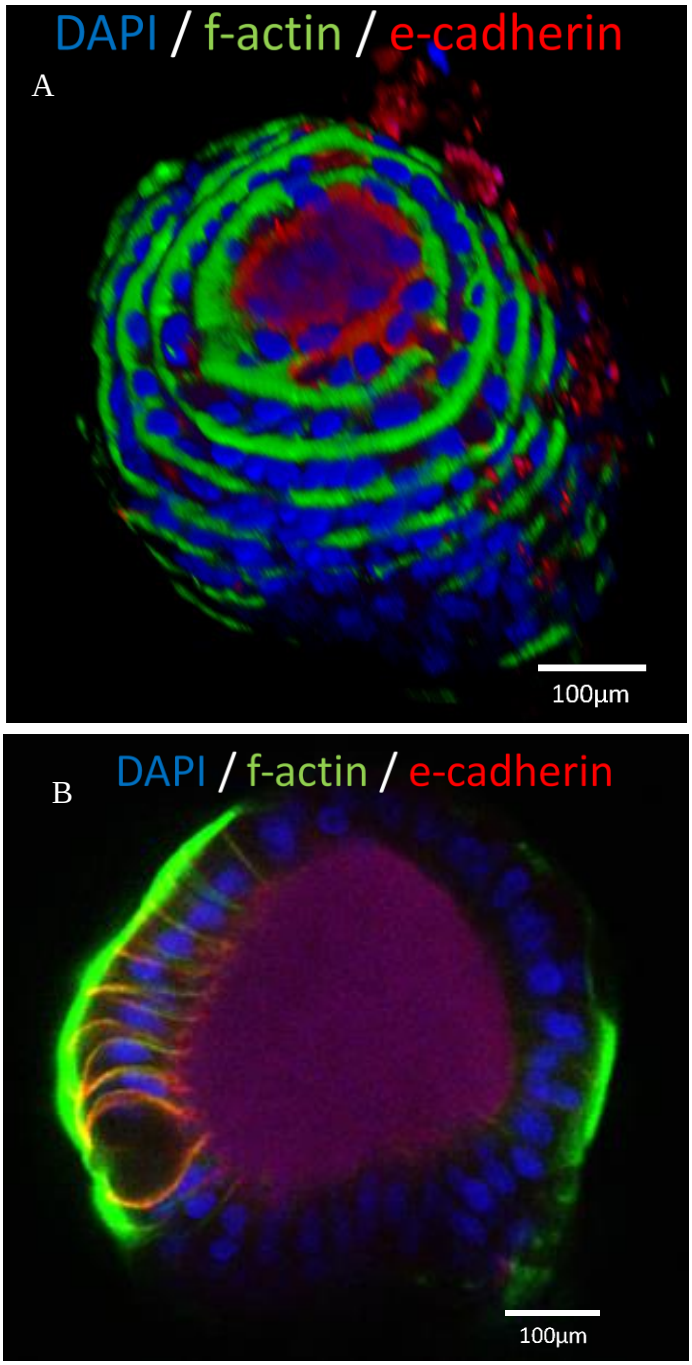

Figure 36. Single Villus on Silk Hydrogel Covered by Enteroids. Confocal microscopy. The tips of the silk hydrogel scaffolds, coated with collagen type I, were seeded with ileum enteroids. These images were acquired using DAPI (blue), f-actin (green), and e-cadherin (red) staining. A) Top view of single villus. Cell nuclei were seen throughout the surface of the feature. There were rings of actin and cells with tight junction formation on the villus. B) Cross section of respective villus. The cells were polarized. The tight junction formation between the cells was seen more clearly. In addition, the actin formation was seen around the feature and on the outer surface of the cells.

5.4.3 Increasing the Coverage of Enteroids on Featured Scaffolds

After the initial seeding of enteroids on the silk hydrogel scaffolds, we saw the lack of enteroid coverage throughout the scaffold. We tried 2 methods to increase the confluency of the enteroids on the featured scaffolds. The first method involved a longer time for proliferation. The second method involved the use of a poly-L-lysine coating (1mg/mL).

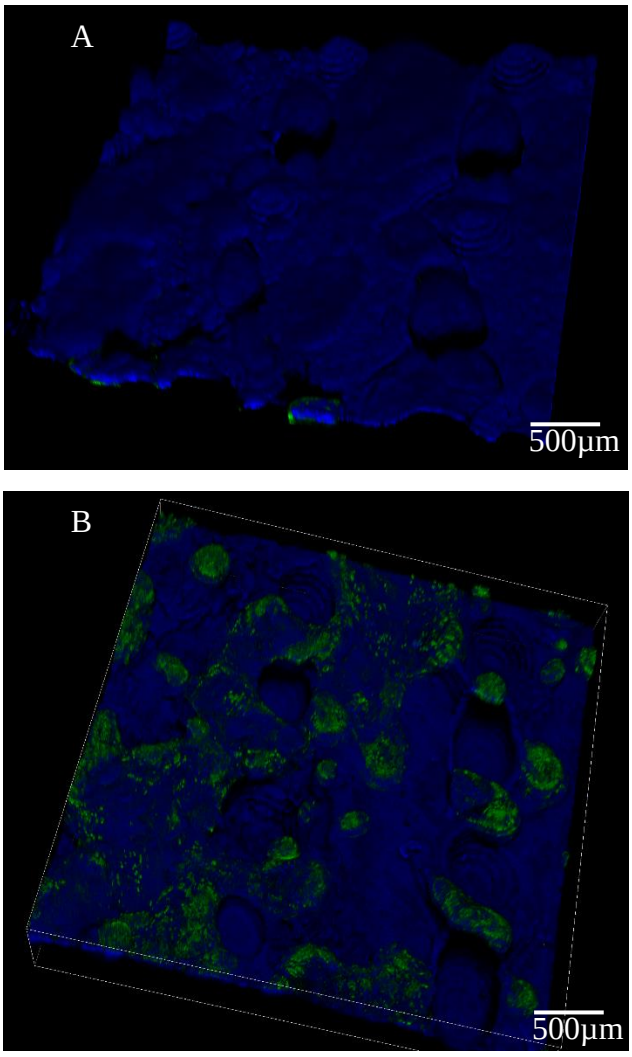

Figure 37. Coverage of Cells after 2 Weeks of Proliferation. Confocal microscopy. The scaffolds were seeded with ileum enteroids. These images were acquired using DAPI (blue). These images were acquired using DAPI (blue). A) View of the bottom of the crypts. The enteroids proliferated into the crypts and covered the area around the features. B) View of the overall scaffold. The full coverage of the surface could be seen even on areas of the scaffolds with and without features.

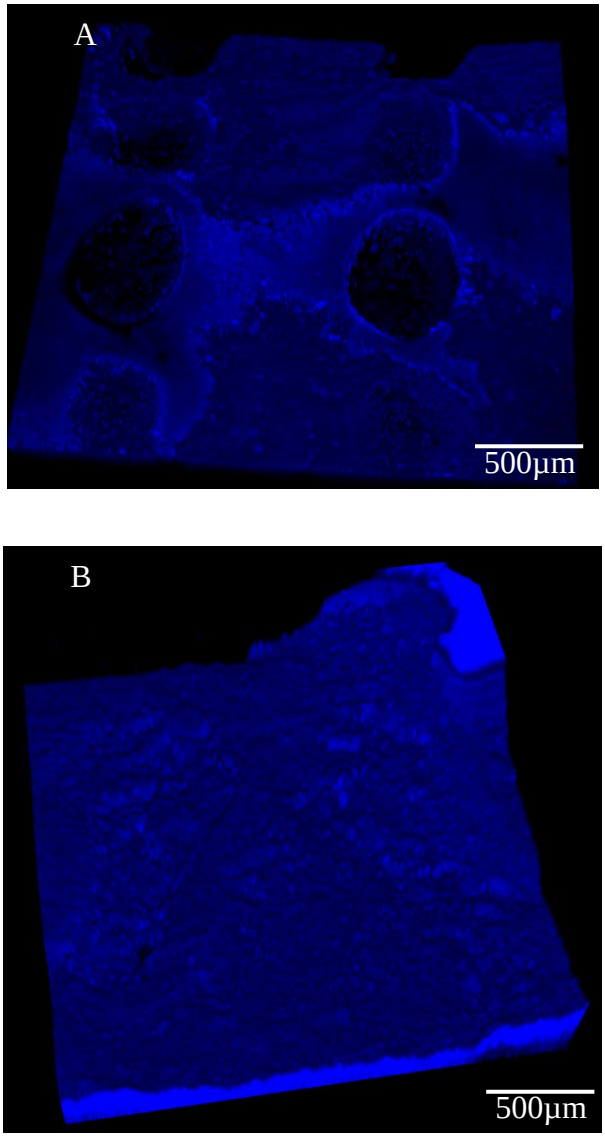

Figure 38. Coverage of Cells Using Poly-L-Lysine Coating. Confocal microscopy. The scaffolds were seeded with ileum enteroids and proliferated for 2 weeks. These images were acquired using DAPI (blue). A) View of the crypts. The enteroids proliferated into the crypts and covered the area around the features. B) View of the overall scaffold. The full coverage of the surface could be seen even on areas of the scaffolds without features.

6. Discussion

6.1. Silk sponges can be fabricated as potential scaffolds for the small intestinal model

The main concern with the silk sponges was the porosity of the material. The pores in general were much larger than the average cell size, which made the replication of the features of self-renewal difficult. The pores were approximately 30µm-150µm (Figure 31). However, by coating the material with silk film, there was a significant reduction in the pores on the surface (Figure 33). The surface was more similar to the silk hydrogel surface (Figure 32). This would allow for co-cultures as the sponge bulk could also be seeded similar to the previous silk intestinal model made by Chen et al. [4,25]. However, with the additional film coating, the self-renewal feature seen in the intestinal epithelium could also be replicated.

6.2. Reproducibility of features using the molding process described to create featured silk hydrogels or film-coated silk sponges

In general, using the 3D printer to create peaks and wells as features was possible. The peaks were made as expected and matched the original computer generated designs. However, the wells had distorted shapes, typically tilted cylindrical cones that were smaller than expected. The features were consistent as long as the diameter of the features exceeded 500µm. The villi features, which had varying heights and shapes, were not always consistent likely due to the 300µm diameter of the features (Figure 18B). The resulting hydrogels with 500µm diameter features (Figure 21 and 23) were more consistent and cone shaped compared to the resulting hydrogels with 300µm diameter

features (Figure 20). Also seen in these molds were the slight tilt of the wells. As the villi features contribute mainly to intestinal function, the peaks ended up becoming the villi in the final scaffolds due to the replicability of their design and printing [44].

There were three methods of fabrication for the silk scaffolds that were considered. The first method used a machined wax negative mold to construct villi features. The second method used a negative mold to construct villi and crypts on film-coated silk sponges. The third method used a positive mold to construct villi and crypts on silk hydrogels and film-coated silk sponges.

6.2.1. Machined wax molds to create silk hydrogels

The machined wax molds were mostly according to the design. The diameter of the features matched and the depth of the villi were as expected. However, the geometry of the features resulted in flat peaks rather than rounded peaks. The molding process worked out accordingly as we were able to see a clean transition of material from one mold to the next. The epoxy was able to copy the features from the wax mold well even with a coating in between (Figure 15). There was another limitation in that the epoxy material would have an oily coating. This was likely amine blush, which caused the PDMS to not cure at every point in contact with the epoxy material [45]. Amine blush typically is induced in low temperature, high humidity conditions [45]. There were attempts to remove the amine blush, such as rinsing with detergent or keeping the epoxy in a vacuum while it cured. In the end, the material was switched to Ecoflex 00-35 rubber, due to its ability to replicate the features well from the wax mold and its compatibility with the PDMS

material. The PDMS was also capable of replicating the epoxy features well (Figure 16). The final silk hydrogel scaffold with villi had replicated the features from the original wax mold throughout the molding process (Figure 17). However, due to the limitations of the machining, this was not the most ideal method for fabrication. The machining of the features was dependent on the bit being used to mill the wax. Thus, for smaller resolutions, if the feature desired was not possible with a commercially available bit, a custom bit had to be fabricated, which can be costly and inaccessible. In addition, the machining of such fine features to create both villi and crypts was not possible. In order to create peaks, the machine would need to carve at the wax block and destroy other carved out features. A method of resolving this issue could be to mill out the holes and use a molding material for the second step that can be milled. This would allow for the holes to be copied as peaks on the second molding material and new holes to be milled to create villi features for the final silk scaffolds. However, this would require an extra step in the molding process and precision milling. Therefore, this method of fabrication using machining was not ideal for creating crypts and villi features on the final silk scaffolds.

6.2.2. Negative resin molds to create film-coated silk sponges

Although the negative resin printed molds were not according to design, the features were consistent. As previously indicated, the peaks were as expected in terms of dimensions and shape. However, the wells had a severely distorted shape that was smaller than the design. Increasing the height of the design increased the depth of the well, which allowed for proper adjustments to be made to the design so the wells would be considered physiologically relevant.

In the case of the negative resin printed mold, the peaks came out well (Figure 25). However, since the final scaffold was inverted, the peaks on the original mold were the crypts and the wells on the original mold were the villi. When trying to replicate the negative mold directly using a film-coated silk sponge, the features were nearly non-existent (Figure 26). Many of the features tore and stuck to the printed mold. There were holes left in the film coating as a result. With holes in the coating, the pore sizes of the sponge became an issue as any cells seeded on the scaffold would proliferate into the bulk through the holes rather than the surface. In addition, due to the inversion of the features, the crypts ended up being larger than the villi, which was not physiologically accurate to humans [7]. Some improvements could be made by increasing the size of the features in the design as long as the dimensions remain within human relevancy.

In the case of the negative resin printed 3D mold, the peaks came out well (Figure 29). Again, the wells were not according to the design and were smaller than expected; the shape was also distorted. When trying to replicate the negative mold directly using a film-coated silk sponge, the features did not come out well (Figure 30). The film coating did not transfer to the final scaffold (Figure 30B). The pores seen were clearly from the sponge material. The features did not come out well, as many of the features were smaller or not apparent on the final scaffold. Due to the large pore sizes, the cells would likely proliferate through the bulk. Some improvements could be made by adding a release agent to the resin mold to aid the removal of the film coating and fabricating the silk film

coating after the silk sponge. Softening the film-coating with glycerol could also aid the removal process.

The transfer from negative resin mold to silk sponge was inaccurate and did not retain the features well. In addition, the film coating was destroyed in the removal process, which made the final scaffolds unsuitable for seeding. This method of fabricating silk sponges was not ideal.

6.2.3. Positive resin molds to create silk hydrogels or film-coated silk sponges with walls

Although the negative resin printed molds were not according to design, the features were consistent. As previously indicated, the peaks were as expected in terms of dimensions and shape. However, the wells had a severely distorted shape that was smaller than the design. Increasing the height of the design increased the depth of the well, which allowed for proper adjustments to be made to the design so the wells would be considered physiologically relevant. As the peaks result in the villi and the wells result in the crypts, the shape of the wells were not too significant as they were consistent. In a previous report, the fabrication method using the positive resin mold was established as sufficient for replicating features on silk hydrogels and film-coated silk sponges.

In order to improve the efficiency of the seeding of the enteroids, walls were added on the scaffolds. Initial methods of seeding using surface tension resulted in the enteroids adhering initially to the tips. Thus, to improve the coverage of the initial seeding and

enhance the amount of enteroids seeded, we created walls around the scaffolds so we would not have to rely on the surface tension. The addition of a wall around the silk hydrogels did not interfere with the molding process as the features came out well (Figure 23). Thus, the molding process beginning with the positive resin mold replicated the topographical features of the small intestines on the flat silk hydrogel.

The addition of a wall around the film-coated silk sponge did not interfere with the molding process as the features came out well (Figure 24). Thus, the molding process beginning with the positive resin mold replicated the topography of the small intestines on the flat film-coated silk sponge.

6.3. Modeling human small intestines using enteroids seeded on featured silk hydrogel scaffolds

6.3.1. Demonstration of adherence and proliferation of enteroids

To ensure the proper collagen coating could be applied to the silk scaffolds, Caco-2 cells were first tested on the featured silk scaffolds. Using Caco-2, we were able to see adherence to and coverage of the villi after 1 week of proliferation using a 50μg/cm^2 coating of collagen type I (Figure 34).

After creating featured flat silk hydrogels with villi and crypts, ileum enteroids were seeded. After seeding the enteroids and proliferating them for 7 days, the villi were completely covered. The enteroids were capable of adhering to the collagen-coated silk hydrogel scaffolds and proliferated throughout the scaffold, forming confluent layers on

the villi features (Figure 35). Using DAPI (blue) staining, the presence of the enteroids' nuclei was seen on the features. Following the 7 days of proliferation, the enteroids were differentiated for 5 days. Using e-cadherin (red) staining, tight junction formation could be visualized throughout the features. Using f-actin (green) staining, the apical brush border membrane could be visualized as rings around the villi. The DAPI staining seen in Figure 35 was similar to the DAPI staining in Wang et al.'s collagen-enteroid model [18]. The enteroids surrounded the villi features and proliferated around the feature, rather than throughout. Thus, silk hydrogels were capable of supporting the proliferation and differentiation of enteroids.

Others have used featured scaffolds with Caco-2 cells as their intestinal model. Compared to Yu Jiajie et al.'s collagen model and Costello et al.'s PLGA model, the coverage of the actin and cell nuclei were similar to our model [46]. The tight junction formation, cell nuclei proliferation, and f-actin formation seen in Kim & Ingber's gut-on-a-chip model was also similar to our model [16]. The tight junction formation was seen on top of the villi, similar to Kim & Ingber. In addition, the cells and actin covered the villi, showing the similarity in the development of the intestinal model. The collagen model has been used to evaluate drug permeability, suggesting our model could also be potentially used for testing drug treatments. Also, the PLGA model has been used to evaluate the therapeutic potential of various probiotics. The model evaluated the adhesion and invasion of *Salmonella* and *Pseudomonas* and the therapeutic potential of *Lactobacillus* and *E. coli* suggesting our model may be capable of incorporating bacteria seen in the human intestines [13]. Our featured silk hydrogel scaffolds with villi and crypts

had similar tight junction formation, f-actin linings, and cell coverage to other intestinal models, suggesting our model could perform similar intestinal functions if evaluated in the context of drug delivery or treatments.

6.3.2. Demonstration of polarization on villi features of enteroids

In addition to adherence and proliferation, polarization of the enteroids were seen on the villi features. The enteroid nuclei seen in Figure 36 were not lying flat on the feature. The cells were polarized, sticking up on the feature. This polarization is a common feature of epithelial cells and contributes to the transport functions in the intestines [47]. Other intestinal models, such as the collagen model and the PLGA model, have shown cross sections of the villi with similar patterning [3,46]. In addition, the formation of the brush border enzyme was visualized (Figure 36). Similar to the human intestines, the brush border lies on the outside of the cells on the villus features [48]. This further supported the idea that our silk hydrogel model could be used to evaluate intestinal functions as a physiologically relevant model to humans.

6.3.3 Demonstration of enhanced coverage after 2 weeks of proliferation and the use of poly-L-lysine coating

Although there was full coverage of the enteroids on the villi features from previous data, there was a lack of coverage of the crypts in the scaffolds. We were able to see the full coverage of cells in the crypts after 2 weeks of proliferation (Figure 37). Compared to the previous scaffolds which only covered the villi, the crypts also had a confluent layer of cells. In addition, using the additional coating of poly-L-lysine improved the coverage of

enteroids on the scaffolds after 2 weeks of proliferation (Figure 38). The coverage of cells was seen on surfaces without features, indicating confluent coverage of the featured scaffolds.

7. Conclusions

Millions of people worldwide are affected by intestinal diseases [1]. In addition, many pharmacological treatments in general use oral delivery, which involves the gastrointestinal tract. Clinical trials are expensive and time-consuming, making the process for developing therapeutic means to treat intestinal diseases limited. However, current intestinal models are imperfect in their ability to replicate the functions and structures of the human intestines. The development of non-human models can increase the efficiency and decrease the cost of treatments for these intestinal diseases. The parameters and conditions in an animal model are difficult to control and can result in uncertainty in terms of human physiological relevance [2]. *In vitro* intestinal systems are also lacking in their physiological relevance. Many co-culture and 2D model systems have been developed, but lack significant features of the human intestines such as topographical features and the ability for self-renewal, which are crucial for human small intestinal functions.

Many *in vitro* 3D intestinal models have been constructed in order to establish physiological relevance to humans. These models vary in the material used, the properties evaluated, and the physiological relevance. However, the silk intestinal model previously made by Chen et al. has properties similar to the human intestines [4]. The model used silk as the scaffolding material, which has excellent properties to support tissue systems. The

resulting model had a co-culture system with myofibroblasts, absorptive cells, and goblet cells, a double layer of mucus, a gradient in oxygen tension, polarized epithelial cells, columnar structures, and the potential to host bacteria in the lumen [4]. The model was further improved with the incorporation of enteroids, small intestinal organoids [25]. The system had characterized the four major epithelial cell types, tight junction formation, microvilli polarization, digestive enzyme secretion, gradient of oxygen, and an antibacterial response to *E. coli* infection. However, the model, like many other *in vitro* systems, lacked the ability to demonstrate self-renewal.

It was shown that introducing intestinal topography into *in vitro* models could influence the formation of cells into physiologically relevant tissue with functions similar to the human intestines [5,49,50]. In this body of work, we have reported on the incorporation of crypts and villi as part of the silk intestinal model to further enhance the physiological relevance of the model. We aimed to recreate the effect of self-renewal by incorporating the combination of enteroids and topography. We have established a method of fabrication for these features, based on previous work that is commonly used in intestinal models to create the microtopography. We have demonstrated that 3D printing can be used as a method for creating villi and crypts topography with physiologically relevant shapes and dimensions. We have also demonstrated that these features could be replicated on both silk hydrogels and film-coated silk sponges, indicating silk's ability to act as a scaffold for this model. In addition, we have shown that using a positive resin mold for fabrication of crypts and villi was better than the negative resin mold and the

machined wax mold. With the established method of fabricating featured silk scaffolds, we modeled human small intestines using enteroids.

As enteroids are intestinal crypts-derived stem cells, the differentiation of these cells into the four main intestinal epithelial cell types was possible. Incorporating these cells into the proper niche would allow the enteroids to proliferate and differentiate similarly to the small intestines. After seeding enteroids of the featured scaffolds, we were able to see adherence and proliferation of enteroids to the silk scaffolds. The villi and crypts features were able to be covered after 2 weeks of proliferation. We were also able to differentiate the enteroids and see tight junction formation, the presence of an apical brush border enzyme, and polarized epithelial cells on the villi. The pattern of cells seen in our model was similar to others, suggesting our silk model is capable of evaluating intestinal functions in the context of drug delivery and developing treatments.

8. Future Directions

Most of this work has provided initial evidence for the enhanced formation of the intestinal lining in the *in vitro* silk intestinal model. While we established a novel method for making the villi and crypts topography on the silk materials and demonstrated the compatibility of the system with enteroids, this improved model has yet to be characterized quantitatively. It is important to quantify the presence of the four major intestinal epithelial cell types as this will demonstrate the model's physiological relevance. In addition, another key feature that needs to be quantified is the tight junction formation. Although visibly, the tight junctions formed, there should be a comparison to

other models or to previous silk models to see if this new system is an improvement. Mucus layer formation should have also been measured as the mucus layer thickness also plays a role in the absorptive capabilities of the intestines. In addition, the silk scaffolds also need to be evaluated mechanically. The stiffness of the scaffolds has not been considered in terms of their relevance to the human intestines, which can be an important consideration for creating a physiological relevant human intestinal model.

In addition to quantification, there were plans to construct a 3D scaffold with features, similar to the previous system. This would likely create a more representative intestinal niche and further enhance the physiological relevance to human intestines, making it a crucial property to be included as part of the future works. Another aspect of the scaffold that needs to be improved is the density of the features. The density of the features needs to be increased so the spacing between the villi and crypts features are more similar to the human intestines. Another consideration for increasing the physiological relevancy of the model is changing the method of fabrication to copy existing animal intestinal features. This could be done similarly to a model done by Koppes et al., which used porcine intestines to recreate intestinal features on PDMS [51]. However, we could incorporate these porcine features onto silk scaffolds instead. In addition, improvements could be made to the scaffolds by making the villi features hollow. This would allow for the perfusion of nutrients and signaling factors from underneath the features as well.

Another significant feature that should be included as the next steps in the model is the biochemical gradient seen in the intestinal niche. Common signaling factors seen in the

small intestines should be incorporated as a gradient into the model in order to enhance the proliferation in the crypts and differentiation on the villi. This would aid in the process of establishing a self-renewing system, which is the crucial for intestinal function.

Once the system has been established, comparing our model to other 2D and 3D *in vitro* models, such as Chen et al.'s model would be important [4]. Comparing the properties between the existing model in the lab and the newly devised model would be crucial in ensuring that this system is improved. One aspect for comparison could be to compare the features created using a screw in the original silk model to the features created using 3D printing in this proposed model. In addition, comparing the tight junction formation, brush border formation, mucus layer thickness, and other characteristics of the intestinal epithelium would be crucial as well.

In order to make sure this *in vitro* small intestinal model is relevant and capable of being used for studies, intestinal microbiota and diseases should be applied to this system. As other *in vitro* models have established, incorporating *E. coli* bacteria or probiotics could aid in demonstrating the physiological relevance of this model to human intestines. If this model is established as an appropriate system to evaluate the changes and responses of the human intestines, it could be used in the future as a drug screening system and reduce the cost of pharmacological oral treatments.

Although there are still many ways to enhance the described *in vitro* silk small intestinal system, we have demonstrated a method to fabricate villi and crypts topography on silk and established the compatibility between enteroids and silk biomaterials. Using positively printed resin molds, we were able to create physiologically relevant villi and crypts in the silk scaffolds. We demonstrated the ability of enteroids to proliferate and adhere to the features, particularly the villi. The features were completely covered by cells, in addition to the presence of actin filaments and tight junctions. The polarization of the cells was also evident on the villi, similar to the human epithelium. With further developments, this model will likely be capable of in vitro modeling for disease studies, functional understanding, and drug discovery.

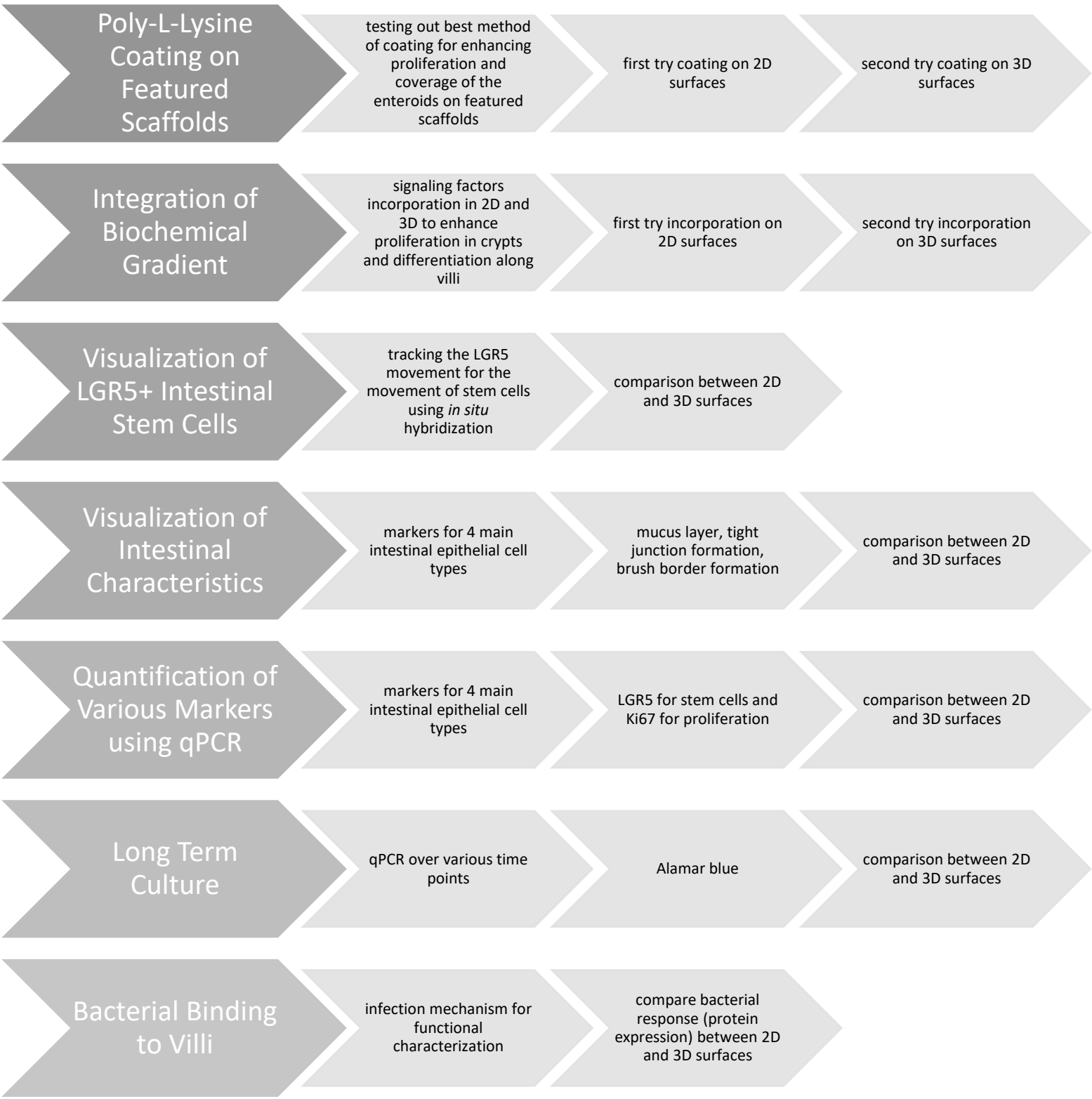

Figure 39. Diagram of the Next Steps for Improving the Intestinal Model. The first arrow in each row indicated the major idea of what needs to be done. The rest of the arrows in the row are descriptions of various things that need to be associated with that major idea.

9. Appendices

A) Wax Mold Drawing

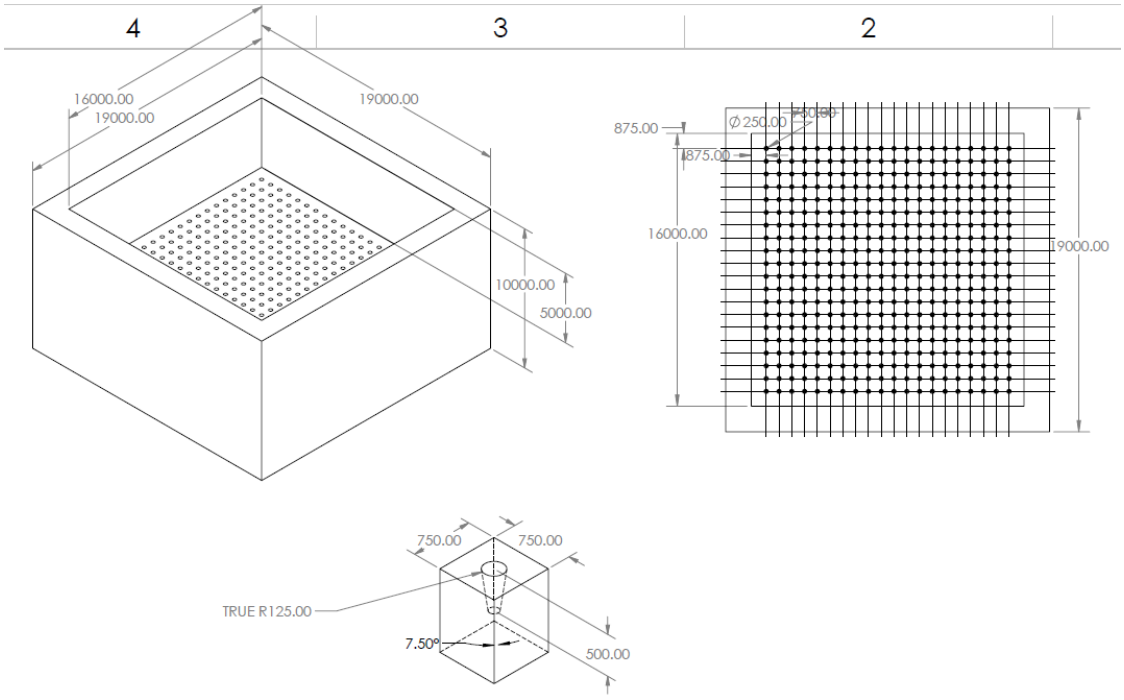

B) 800um Villi 700um Crypts Negative Resin Mold Drawing

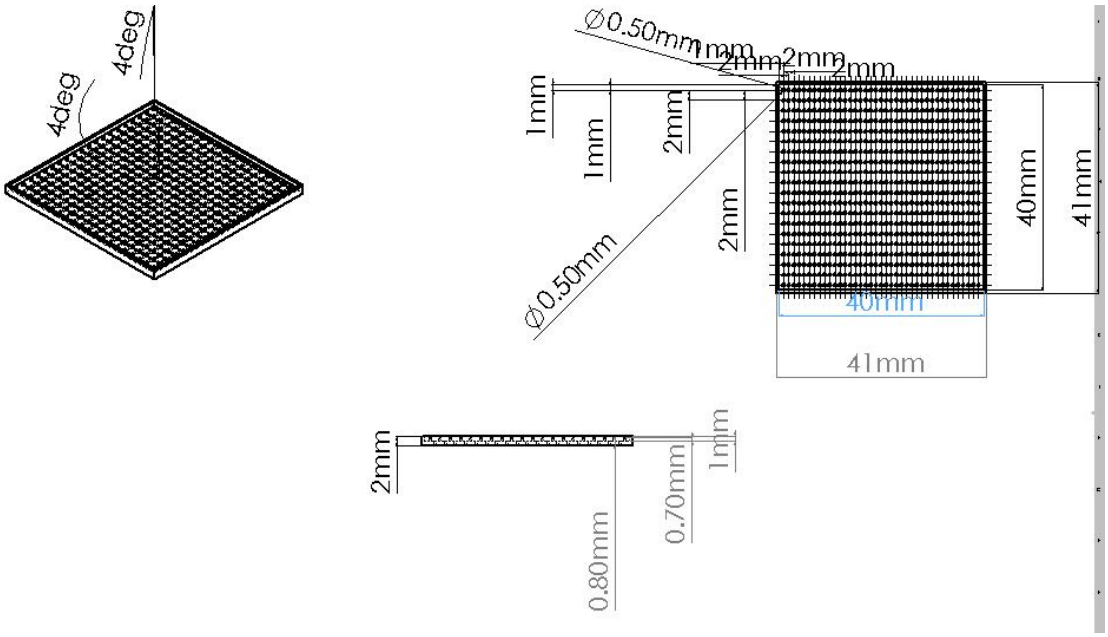

C) 800um Villi 700um Crypts Positive Resin Mold with Walls Drawing

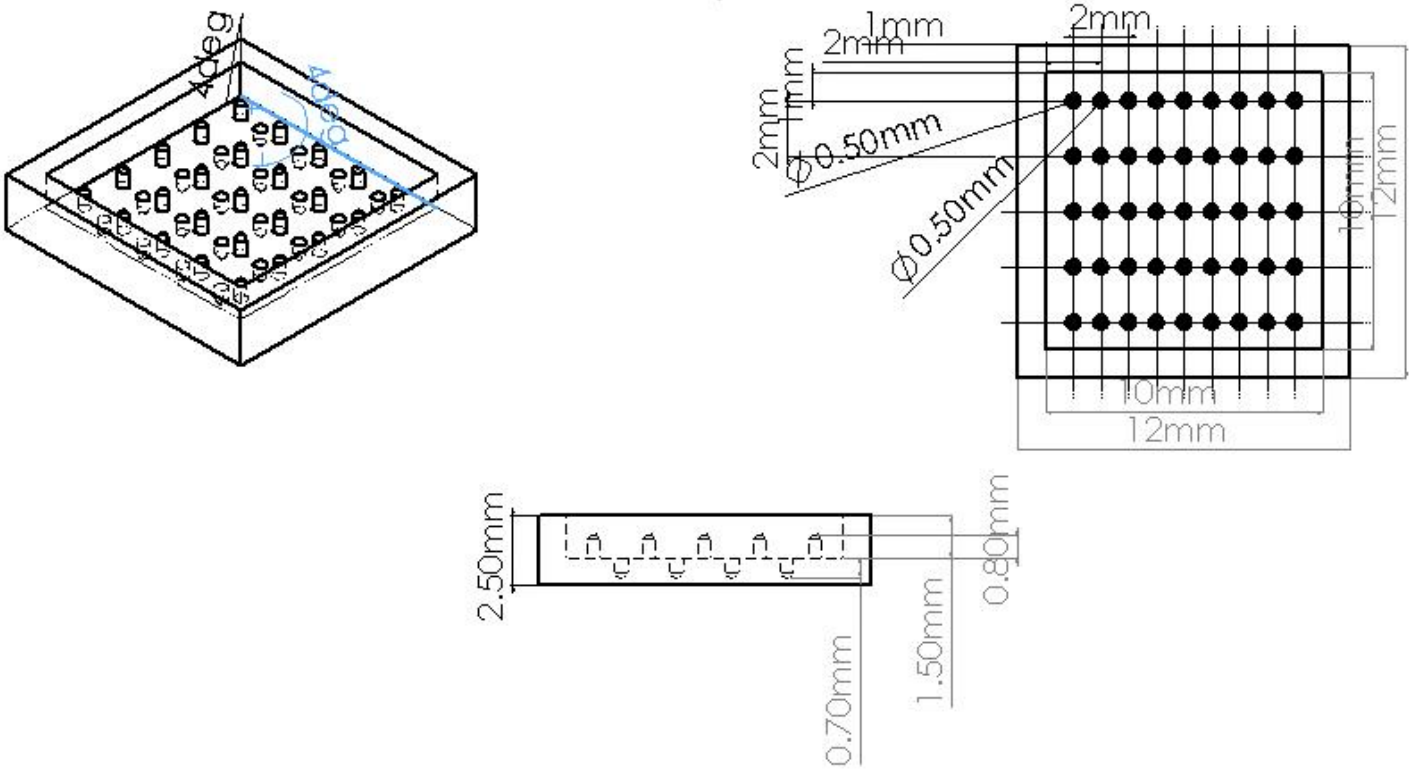

D) 800um Villi 700um Crypts 3D Cylinder Negative Resin Mold

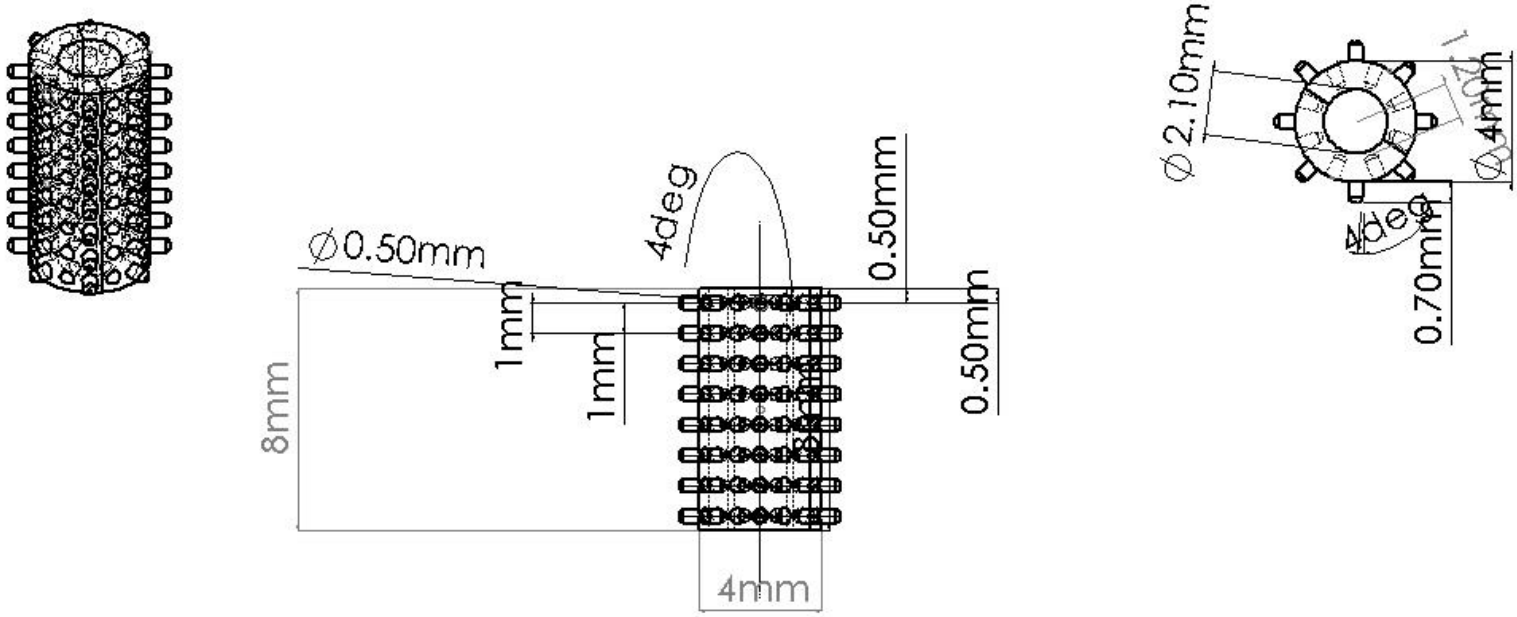

10. References

1. Burisch J, Munkholm P. The epidemiology of inflammatory bowel disease. Scand J Gastroenterol. 2015 Aug 3;50(8):942–951.

2. Jiminez JA, Uwiera TC, Douglas Inglis G, Uwiera RRE. Animal models to study acute and chronic intestinal inflammation in mammals. Gut Pathog [Internet]. 2015 Nov 10 [cited 2017 Feb 14];7. Available from: http://www.ncbi.nlm.nih.gov/pmc/articles/PMC4641401/ PMCID: PMC4641401

3. Costello CM, Hongpeng J, Shaffiey S, Yu J, Jain NK, Hackam D, March JC. Synthetic Small Intestinal Scaffolds for Improved Studies of Intestinal Differentiation. Biotechnol Bioeng. 2014 Jun;111(6):1222–1232. PMCID: PMC4233677

4. Chen Y, Lin Y, Davis KM, Wang Q, Rnjak-Kovacina J, Li C, Isberg RR, Kumamoto CA, Mecsas J, Kaplan DL. Robust bioengineered 3D functional human intestinal epithelium. Sci Rep. 2015 Sep 16;5:13708.

5. Wang L, Murthy SK, Barabino GA, Carrier RL. Synergic effects of crypt-like topography and ECM proteins on intestinal cell behavior in collagen based membranes. Biomaterials. 2010 Oct;31(29):7586–7598. PMID: 20643478

6. Openstax. Anatomy and Physiology [Internet]. Openstax; 2013. Available from: https://opentextbc.ca/anatomyandphysiology/

7. The Small Intestine | Boundless Anatomy and Physiology [Internet]. [cited 2018 Feb 2]. Available from: https://courses.lumenlearning.com/boundless-ap/chapter/the-small-intestine/

8. Dalal J, Radhi M. Intestinal Stem Cells: Common Signal Pathways, Human Disease Correlation, and Implications for Therapies [Internet]. International Scholarly Research Notices. 2013 [cited 2018 Jan 30]. Available from: https://www.hindawi.com/journals/isrn/2013/372068/

9. Crosnier C, Stamataki D, Lewis J. Organizing cell renewal in the intestine: stem cells, signals and combinatorial control. Nat Rev Genet. 2006 May;7(5):349–359.

10. Wang L, Murthy SK, Fowle WH, Barabino GA, Carrier RL. Influence of micro-well biomimetic topography on intestinal epithelial Caco-2 cell phenotype. Biomaterials. 2009 Dec;30(36):6825–6834.

11. Muñoz J, Stange DE, Schepers AG, van de Wetering M, Koo B-K, Itzkovitz S, Volckmann R, Kung KS, Koster J, Radulescu S, Myant K, Versteeg R, Sansom OJ, van Es JH, Barker N, van Oudenaarden A, Mohammed S, Heck AJR, Clevers H. The Lgr5 intestinal stem cell signature: robust expression of proposed quiescent "+4" cell markers. EMBO J. 2012 Jul 18;31(14):3079–3091. PMCID: PMC3400017

12. Wang Y, Kim R, Hinman SS, Zwarycz B, Magness ST, Allbritton NL. Bioengineered Systems and Designer Matrices that Recapitulate the Intestinal Stem Cell Niche. Cell Mol Gastroenterol Hepatol [Internet]. 2018 Jan 15 [cited 2018 Jan 30];0(0). Available from: http://www.cmghjournal.org/article/S2352-345X(18)30014-6/fulltext

13. Costello CM, Sorna RM, Goh Y-L, Cengic I, Jain NK, March JC. 3-D Intestinal Scaffolds for Evaluating the Therapeutic Potential of Probiotics. Mol Pharm. 2014 Jul 7;11(7):2030–2039.

14. Hubatsch I, Ragnarsson EGE, Artursson P. Determination of drug permeability and prediction of drug absorption in Caco-2 monolayers. Nat Protoc. 2007 Sep;2(9):2111–2119.

15. Noben M, Vanhove W, Arnauts K, Santo Ramalho A, Van Assche G, Vermeire S, Verfaillie C, Ferrante M. Human intestinal epithelium in a dish: Current models for research into gastrointestinal pathophysiology. United Eur Gastroenterol J. 2017 Dec;5(8):1073–1081. PMCID: PMC5721984

16. Kim HJ, Ingber DE. Gut-on-a-Chip microenvironment induces human intestinal cells to undergo villus differentiation. Integr Biol. 2013 Aug 19;5(9):1130–1140.

17. Barrila J, Radtke AL, Crabbé A, Sarker SF, Herbst-Kralovetz MM, Ott CM, Nickerson CA. Organotypic 3D cell culture models: using the rotating wall vessel to study host–pathogen interactions. Nat Rev Microbiol. 2010 Nov;8(11):791–801.

18. Wang Y, Gunasekara DB, Reed MI, DiSalvo M, Bultman SJ, Sims CE, Magness ST, Allbritton NL. A microengineered collagen scaffold for generating a polarized crypt-villus architecture of human small intestinal epithelium. Biomaterials. 2017 Jun 1;128:44–55.

19. Wang Y, Kim H-J, Vunjak-Novakovic G, Kaplan DL. Stem cell-based tissue engineering with silk biomaterials. Biomaterials. 2006 Dec;27(36):6064–6082.

20. Altman GH, Diaz F, Jakuba C, Calabro T, Horan RL, Chen J, Lu H, Richmond J, Kaplan DL. Silk-based biomaterials. Biomaterials. 2003 Feb;24(3):401–416.

21. Partlow BP, Hanna CW, Rnjak-Kovacina J, Moreau JE, Applegate MB, Burke KA, Marelli B, Mitropoulos AN, Omenetto FG, Kaplan DL. Highly tunable elastomeric silk biomaterials. Adv Funct Mater. 2014 Aug 6;24(29):4615–4624. PMCID: PMC4225629

22. Abbott RD, Kimmerling EP, Cairns DM, Kaplan DL. Silk as a Biomaterial to Support Long-Term Three-Dimensional Tissue Cultures. ACS Appl Mater Interfaces. 2016 Aug 31;8(34):21861–21868.

23. Georgakoudi I, Tsai I, Greiner C, Wong C, DeFelice J, Kaplan D. Intrinsic fluorescence changes associated with the conformational state of silk fibroin in biomaterial matrices. Opt Express. 2007 Feb 5;15(3):1043–1053.

24. Linden SK, Sutton P, Karlsson NG, Korolik V, McGuckin MA. Mucins in the mucosal barrier to infection. Mucosal Immunol. 2008 Mar 5;1(3):183–197.

25. Chen Y, Zhou W, Roh T, Estes MK, Kaplan DL. In vitro enteroid-derived three-dimensional tissue model of human small intestinal epithelium with innate immune responses. PLOS ONE. 2017 Nov 29;12(11):e0187880.

26. Stinson. Expanding the Utility of Silk Fibroin Microneedles: An Investigation of Device and Fabrication Process Improvements for Transdermal Vaccination and Broader Applications. Tufts Digit Libr. 2017 Feb;

27. Rnjak-Kovacina J, Wray LS, Burke KA, Torregrosa T, Golinski JM, Huang W, Kaplan DL. Lyophilized Silk Sponges: A Versatile Biomaterial Platform for Soft Tissue Engineering. ACS Biomater Sci Eng. 2015 Apr 13;1(4):260–270. PMCID: PMC4426347

28. Zhao S, Chen Y, Partlow BP, Golding AS, Tseng P, Coburn J, Applegate MB, Moreau JE, Omenetto FG, Kaplan DL. Bio-functionalized silk hydrogel microfluidic systems. Biomaterials. 2016 Jul;93:60–70.

29. Mahe MM, Sundaram N, Watson CL, Shroyer NF, Helmrath MA. Establishment of Human Epithelial Enteroids and Colonoids from Whole Tissue and Biopsy. J Vis Exp JoVE [Internet]. 2015 Mar 6 [cited 2017 Mar 30];(97). Available from: http://www.ncbi.nlm.nih.gov/pmc/articles/PMC4401205/ PMCID: PMC4401205

30. Sambuy Y, Angelis ID, Ranaldi G, Scarino ML, Stammati A, Zucco F. The Caco-2 cell line as a model of the intestinal barrier: influence of cell and culture-related factors on Caco-2 cell functional characteristics. Cell Biol Toxicol. 2005 Jan 1;21(1):1–26.

31. Fatehullah A, Tan SH, Barker N. Organoids as an in vitro model of human development and disease. Nat Cell Biol. 2016 Mar;18(3):246–254.

32. Zachos NC, Kovbasnjuk O, Foulke-Abel J, In J, Blutt SE, de Jonge HR, Estes MK, Donowitz M. Human Enteroids/Colonoids and Intestinal Organoids Functionally Recapitulate Normal Intestinal Physiology and Pathophysiology. J Biol Chem. 2016 Feb 19;291(8):3759–3766. PMCID: PMC4759158

33. Sato T, Stange DE, Ferrante M, Vries RGJ, van Es JH, van den Brink S, van Houdt WJ, Pronk A, van Gorp J, Siersema PD, Clevers H. Long-term Expansion of Epithelial Organoids From Human Colon, Adenoma, Adenocarcinoma, and Barrett's Epithelium. Gastroenterology. 2011 Nov;141(5):1762–1772.

34. Noel G, Baetz NW, Staab JF, Donowitz M, Kovbasnjuk O, Pasetti MF, Zachos NC. A primary human macrophage-enteroid co-culture model to investigate mucosal gut physiology and host-pathogen interactions. Sci Rep. 2017 Mar 27;7:45270.

35. Saxena K, Blutt SE, Ettayebi K, Zeng X-L, Broughman JR, Crawford SE, Karandikar UC, Sastri NP, Conner ME, Opekun AR, Graham DY, Qureshi W, Sherman V, Foulke-Abel J, In J, Kovbasnjuk O, Zachos NC, Donowitz M, Estes MK. Human Intestinal Enteroids: a New Model To Study Human Rotavirus Infection, Host Restriction, and Pathophysiology. J Virol. 2015 Dec 17;90(1):43–56. PMCID: PMC4702582

36. Hasan M, Ferguson A. Measurements of intestinal villi non-specific and ulcer-associated duodenitis-correlation between area of microdissected villus and villus epithelial cell count. [Internet]. 1981 [cited 2017 Feb 20]. Available from: https://www.ncbi.nlm.nih.gov/pmc/articles/PMC494386/

37. Bernstein C. Cancer and age related colonic crypt deficiencies in cytochrome c oxidase I. World J Gastrointest Oncol. 2010;2(12):429.

38. Zhao S, Chen A, Revzin A, Pan T. Stereomask lithography (SML): a universal multi-object micro- patterning technique for biological applications. Lab Chip. 2011;11(2):224–230.

39. Qin D, Xia Y, Whitesides GM. Soft lithography for micro- and nanoscale patterning. Nat Protoc. 2010 Mar;5(3):491–502.

40. Jose RR, Brown JE, Polido KE, Omenetto FG, Kaplan DL. Polyol-Silk Bioink Formulations as Two-Part Room-Temperature Curable Materials for 3D Printing. ACS Biomater Sci Eng. 2015 Sep 14;1(9):780–788.

41. Zein I, Hutmacher DW, Tan KC, Teoh SH. Fused deposition modeling of novel scaffold architectures for tissue engineering applications. Biomaterials. 2002 Feb 15;23(4):1169–1185.

42. The Ultimate Guide to Stereolithography (SLA) 3D Printing [Internet]. [cited 2018 Feb 12]. Available from: https://formlabs.com/blog/ultimate-guide-to-stereolithography-sla-3d-printing/

43. Rockwood DN, Preda RC, Yücel T, Wang X, Lovett ML, Kaplan DL. Materials fabrication from Bombyx mori silk fibroin. Nat Protoc. 2011 Sep;6(10):1612–1631.

44. DeSesso JM, Jacobson CF. Anatomical and physiological parameters affecting gastrointestinal absorption in humans and rats. Food Chem Toxicol. 2001 Mar 1;39(3):209–228.

45. Weinmann DJ, Dangayach K, Smith C, Temperature L. Cure Coatings.

46. Yu Jiajie, Peng Songming, Luo Dan, March John C. In vitro 3D human small intestinal villous model for drug permeability determination. Biotechnol Bioeng. 2012 Apr 17;109(9):2173–2178.

47. Organization and execution of the epithelial polarity programme [Internet]. [cited 2018 Apr 10]. Available from: https://www.ncbi.nlm.nih.gov/pmc/articles/PMC4211427/

48. Crawley SW, Mooseker MS, Tyska MJ. Shaping the intestinal brush border. J Cell Biol. 2014 Nov 24;207(4):441–451. PMID: 25422372

49. Hyun Kim S, Chi M, Yi B, Hyun Kim S, Oh S, Kim Y, Park S, Hwan Sung J. Three-dimensional intestinal villi epithelium enhances protection of human intestinal cells from bacterial infection by inducing mucin expression. Integr Biol. 2014;6(12):1122–1131.

50. Yu Jiajie, Peng Songming, Luo Dan, March John C. In vitro 3D human small intestinal villous model for drug permeability determination. Biotechnol Bioeng. 2012 Apr 17;109(9):2173–2178.

51. Koppes AN, Kamath M, Pfluger CA, Burkey DD, Dokmeci M, Wang L, Carrier RL. Complex, multi-scale small intestinal topography replicated in cellular growth substrates fabricated via chemical vapor deposition of Parylene C. Biofabrication. 2016;8(3):035011.